공학석사학위논문

극한 주행 성능 향상을 위한 타이어 슬립 정보 기반 통합 샤시제어 알고리즘

Tire slip based integrated chassis control for enhanced limit handling

2016 년 8 월

서울대학교 대학원

기계항공공학부

좌 은 혁

Abstract

Tire slip based integrated chassis control for enhanced limit handling

Eunhyek Joa

School of Mechanical and Aerospace Engineering

The Graduate School

Seoul National University

This paper presents a tire slip based integrated chassis control (ICC) algorithm of four-wheel drive(4WD)/ electronic stability control(ESC)/electronic controlled suspension(ECS) for enhanced limit handling. The principal objective of the vehicle dynamic control algorithm for limit handling is to enable agile, steady maneuver at the limits and expand vehicle control capability to maximum. In order to achieve this objective, the ICC consists of three layers - a supervisor, an upper level controller, and a lower level controller. The supervisor determines desired vehicle motions based on driver commands to the vehicle. The upper level controller calculated virtual control inputs based on desired vehicle motion. In the lower level controller, the virtual control inputs are optimally coordinated to each chassis module based on tire combined slip for enhanced limit handling. The performance of ICC has been investigated via closed loop simulation and vehicle experiment. To investigate the ICC algorithm at the limits via closed loop simulation, the lateral driver model, which mimics professional drivers, for limit handling has been developed and utilized. In the developed driver model, body side slip angle incorporates into path tracking error in contrast to common path tracking algorithms. It has been shown that the proposed ICC algorithm effectively keeps stability and maneuverability of the vehicle at the limits.

Keyword : Integrated chassis control, Limit handling, Combined tire slip, Tangential error
Student Number : 2014-22505

Table of Contents

Chapter 1

Introduction

1.1. Study Background

To enhance the vehicle agility, maneuverability, and stability, various chassis systems –Anti-skid Brake System(ABS), Electronic Stability Control(ESC), Electronic Control Suspension(ECS), and Active Roll System(ARS)– are developed. Moreover, drivetrain and chassis control are combined to improve the controllability, such as Traction Control(TCS) and Four Wheel Drive(4WD). The individual chassis systems are effectively enhanced drivability and ride comfort. The individual chassis systems have been deployed in individual sensors and actuators. This decentralized system is quite common for need to design chassis modules for options. Nowadays, these individual chassis modules become standard features and doors for system centralization are opened.

Without centralization, the individual chassis systems with individual logic can violate other systems' objectives to achieve their own objectives. Thus, there are a number of approaches to integrate each chassis system into one integrated system to effectively improve maneuverability and stability of the vehicle. Nowadays, to guarantee larger stability region and increase vehicle maneuverability, understanding vehicle dynamics at the limits and then designing the vehicle dynamics controller for limit handling is emerged.

In the previous researches [1-3], to gain an insight into the utilization of the vehicle chassis control at the limits, an optimization tool is utilized. Olofsson et al. [1] investigated vehicle maneuvers to cope with different road conditions by solving the time-optimal problem. The solution of an optimal problem could provide guidance regarding how to control the chassis module; however, the solution cannot be directly implemented in real-situations because the optimization could violate real-time constraints. To satisfy real-time constraints and produce similar performance to the optimal solution, some previous researches [2, 3] suggested not only the optimal solution from the optimization, but also the real-time, sub-optimal solution. Edréna et al. [2] suggested an active suspension control algorithm for decreased braking distance. Castro et al. [3] recommended torque vectoring on each wheel for minimizing travelled time. In the previous research [3], a sub-optimal, real-time solution, which basically distributes the longitudinal force as proportional to the vertical force of each tire, was shown to produce similar

performance to the offline optimal solution at the simulation level. However, this rule-based, sub-optimal solution may not deal with unmodelled dynamics, parameter uncertainties and disturbance in real situations.

There are multiple researches on a control algorithm at the limits which well utilizes the friction of each tire by minimizing tire workload [4-7]. The tire workload indicates the amount of friction utilization [2] by using longitudinal, lateral, and vertical force. By minimizing the tire workloads of each wheel, the tire is maintained in a stable region at the limits. Li et al. [4] and Song et al. [6] added tire workload at the cost function and modified the longitudinal force distribution. Madhusudhanan et al. [5] kept the tire workload of the front left and right wheel same in order to prevent saturation of the specific tire, while another tire is unsaturated. Wang et al. [7] suggested a log barrier penalty with respect to the tire workload. To command a physically feasible tire force, the actuator constraints of the longitudinal force distribution are the friction circle of each wheel. These constraints constitute major issues of chassis control at the limits because the friction circle should be maximally utilized, while the controller commands the physically feasible solution. The actuator constraints of the previous researches [4, 5, 7] are considered as nonlinear inequality constraints. Song et al. [6] proposed polygonal constraints to apply the constraints for formulating linear optimization. However, these tire workload approaches and tire force constraints require reasonable tire force signals in the longitudinal, lateral, and vertical directions via estimation or measurement tire forces. In the case of tire force estimation, non-equipped and expensive sensors for commercial vehicles could be necessary.

The chassis control should interpret the driver's intention and efficiently cope with various situations. This role is successfully achieved via three layers in previous researches [8-10]. The three layers consist of a supervisor, an upper level controller, and a lower level controller. The supervisor interprets the driver's intention, such as desired yaw rate and acceleration, with the driver command and vehicle state. To track the desired yaw rate and acceleration, an upper level controller determines the virtual control inputs, desired longitudinal force and yaw moment of the vehicle. Finally, the virtual control inputs are efficiently distributed to each actuator by minimizing the cost function.

An appropriate driver model can be used to evaluate the performance of vehicle chassis control systems via computer simulations before vehicle tests which incurs expenses especially at the limits of handling. Thus, to evaluate the performance of the vehicle chassis control algorithm via vehicle-driver closed loop simulations, the driver model at the limits should be developed. For the regeneration of the steering behavior of a professional human driver at the limits of handling, a lateral driver model should follow the desired trajectory with

acceptable accuracy, even when the vehicle skids on the path due to unavoidable body slip angle. Although there are multiple approaches to lateral driver models [11-13] and they are reasonable in normal driving situations, they cannot accurately represent the steering behavior of a professional human driver especially at the limits of handling.

1.2. Purpose of Research

The thesis focus an integrated chassis control for enhanced limit handling by use of tire slip information. A target vehicle chassis control system has four-wheel-drive (4WD) : front/rear traction distribution, electronic stability control (ESC) : four-wheel independent braking, and electronic controlled suspension (ECS) : four independent damping force in vertical direction. To develop integrated control algorithm of 4WD/ESC (Longitudinal chassis module) and ECS (Vertical chassis module) modules, 4WD/ESC integrated algorithm and 4WD/ESC/ECS/ARS (Active Roll Stabilizer) integrated algorithm are studied and validated in simulation level. Consequently, 4WD/ESC/ECS integrated algorithm is developed and investigated via vehicle tests.

The principal concept of the proposed integrated control algorithm for limit handling is to optimally utilize the friction circle of each tire. By adopting this successful scheme, the overall scheme of the proposed integrated control algorithm in this paper consists of three layers, a supervisor, an upper level controller, and a lower level controller. Three layers are enumerated as : 1) a supervisor computes the desired dynamics from vehicle states and driver command; 2) an upper level controller determines the desired force and moment to track the desired state based on the sliding mode controller; and 3) a lower level controller, which is focused on in this paper to achieve limit handling of vehicle, optimally allocates desired force and moment to actuator control commands by minimizing a performance index.

This thesis proposes a novel cost function. The allocation guideline to lead the solution in the vicinity of the sub-optimal solution and the tire saturation penalty to keep the tire stable by monitoring combined slip, unlike the tire workload which monitors the tire forces, are proposed. The performance of the chassis controller is sensitive to the weighting factor of the cost function [4, 5]. Thus, the controller could produce inconsistent performance, which is undesirable for drivers at the limits and in various situations. The allocation guideline can produce a consistent solution at the limits and in various situations, which cannot be achieved by tire workload. Meanwhile, the tire saturation penalty can keep the tire stable even with uncertainties and disturbances, which cannot be dealt with by the allocation guideline. Moreover, tire saturation could substitute for tire workload by

monitoring combined slip, and not tire forces, which are difficult to estimate or measure. This interaction between allocation guideline and tire saturation penalty could enable safe and limit handling of vehicles. The effectiveness of the proposed algorithm is investigated via closed loop computer simulation and vehicle experiments.

Chapter 2

Vehicle Control System

2.1. Vehicle Chassis System

To appropriately control vehicle, especially at the limits, understanding vehicle system is important. Vehicle interacts with environment through four palm size tire contacts and these contacts determine whole x/y/z direction vehicle dynamics. In each tire, longitudinal/lateral/vertical tire forces are exerted to vehicle. Consequently, 12 tire forces determine whole vehicle dynamics.

In conventional vehicle, to control these 12 tire forces, only 2 inputs are used. Steering wheel angle and Pedal signal. Due to its underactuated nature, vehicle cannot be commanded to follow desired trajectory. Sometimes, following the desired trajectory is only way to avoid obstacle. For many decades, these deviations cause severe accidents.

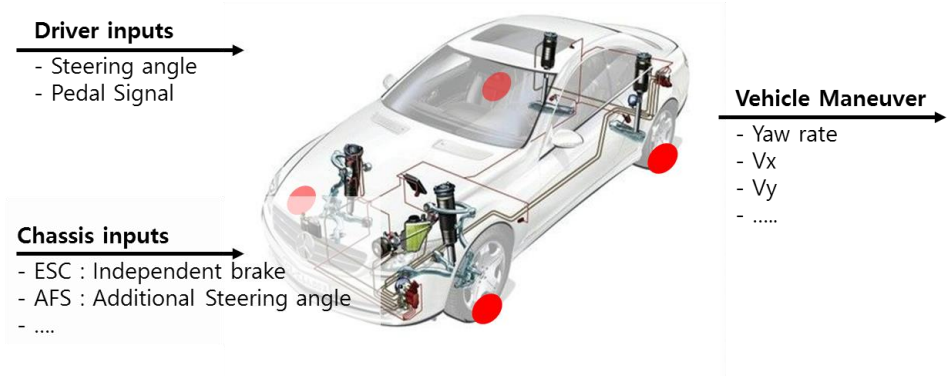

Figure 2.1 Overactuated vehicle chassis system

Nowadays, to overcome these problems and improve vehicle safety, the numerous chassis modules are developed to control 12 tire forces. By equipped these chassis modules, the vehicle system becomes overactuated and prevents accidents. For example, ESC(Electronic Stability Control) can control four brakes independently and generate additional yaw moment. According to NHTSA, adding ESC can prevent at least 5000 annual fatalities.

2.2. Effect of Individual Chassis Modules

This section presents the effect of individual chassis system to each tire force. These chassis modules consists of additional sensors and actuators to control tire force. The individual modules affect longitudinal/lateral/vertical tire force and consequently control wheel/yaw/roll motion of the vehicle.

There are chassis modules. The chassis modules are summarized as

- ESC (Electronic Stability Control) : Four independent brakes
- 4WD (Four Wheel Drive) : Front/rear traction distribution
- AFS (Active Front Steering) : Additional front steering angle
- RWS (Rear Wheel Steering) : Rear steering angle
- ECS (Electronic Controlled Suspension) : Damping coefficient control of four suspension
- ARS (Active Roll Stabilizer) : Auxiliary front/rear roll moment

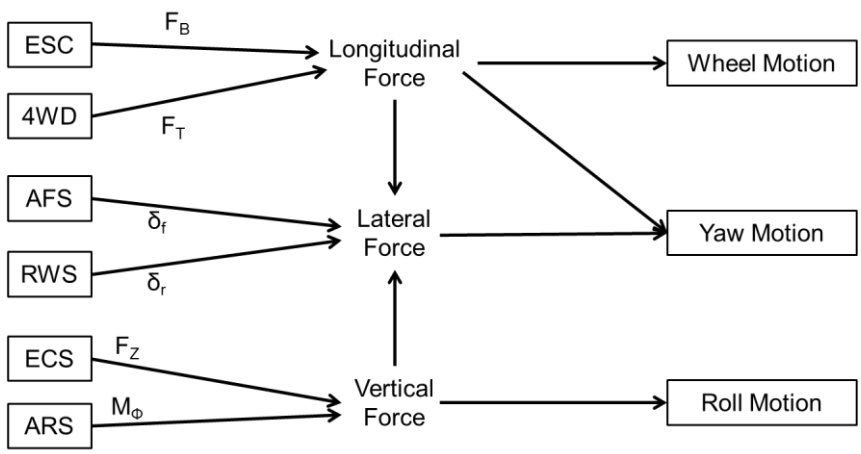

Figure 2.2 Effect of Individual Chassis Modules

ESC and 4WD can directly control longitudinal force of each tire and eventually control wheel motion. However, due to nonlinearity of tire, longitudinal tire force can affect lateral tire force. When longitudinal force exists, lateral tire force decreased even with same side slip angle. Thus, these longitudinal force control modules can affect lateral force and yaw motion eventually.

AFS and RWS can directly control lateral force of each tire. By controlling additional steering angle in front/rear wheel, front/rear lateral tire force can be controlled and yaw motion of the vehicle can be controlled. In particular, RWS system can theoretically eradicate side slip angle of the vehicle.

ECS and ARS can directly control vertical force of each tire and eventually

control roll motion. Similarly, vertical force can affect lateral tire force due to nonlinearity relationship between lateral and vertical tire force. Thus, these longitudinal force control modules can affect lateral force and yaw motion eventually. By use of nonlinearity between lateral and vertical tire force, additional yaw moment can be controlled. [14]

It is best for utilization of all chassis modules, however most of chassis modules are not commercialized. Among the vehicle chassis modules, Electronic stability control (ESC) / four wheel drive (4WD) / Electronic Controlled Suspension (ECS) have been recently equipped in vehicle. Thus, in this research, to achieve limit handling of the vehicle, ESC/4WD are basically chosen for the integrated chassis system among the vehicle chassis modules. In addition, ECS/ARS modules can directly control vertical force and vertical force of each tire is important because it indicate friction limit of each tire. Thus, ESC/4WD/ECS/ARS equipped vehicle are also studied. Finally, ESC/4WD/ECS integrated algorithm are validated via vehicle tests.

Chapter 3

Lateral Driver Model

3.1. Overall Algorithm

The block diagram of the lateral driver model proposed in this study is shown in Figure 3.1. To ensure path tracking ability at the limits of handling, the proposed driver model consists of upper and lower level controllers. Both upper and lower level controllers consist of feedforward and feedback parts. This scheme of the controller well mimics professional human drivers because human drivers also establish a race plan before driving on the track (feedforward) and cope with the track by additional manipulations while driving on the track (feedback).

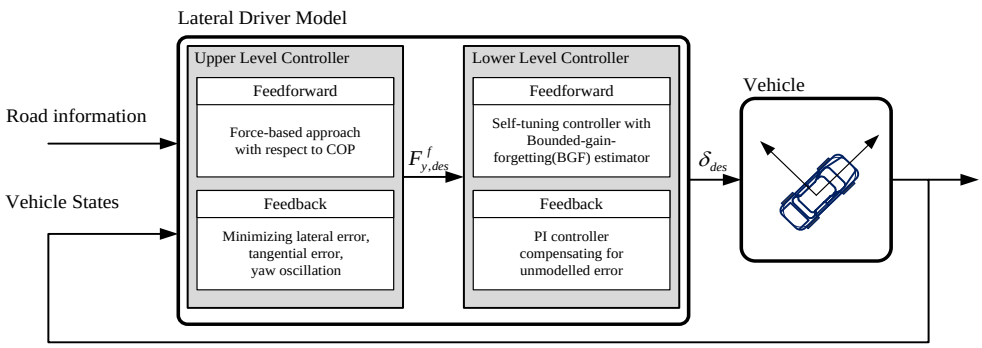

Figure 3.1 Overall block diagram of lateral driver model

In the feedforward part of the upper level controller, force-based steering input which takes advantage of benefits of using center of percussion (COP) is deployed. The effect of the rear tyre is minimized through benefits of COP [15]. Error-modified feedback steering input, whose objective is to minimize yaw error, is replaced to minimize “tangential error”. Steering wheel angle oscillation, which results from recognizing unavoidable body slip angle as heading error, is eliminated through replacing heading error with tangential error.

The control command of the upper level controller is the desired front lateral force, not the steering wheel angle which is available for manipulation in human’s point of view. Therefore, conversion of the desired front lateral force to corresponding steering wheel angle should be conducted in the lower level

controller. In this paper, to achieve the task, the feedforward lower level controller is designed as self-tuning controller with bounded-gain-forgetting(BGF) estimator which convergence is mathematically proved. To formulate a linear parameterization model, a force-based approach using 2 DOF bicycle model and kinematic analysis of steering angle are used. The feedback part of the lower level controller is developed as a PI controller to compensate for the difference between desired lateral force and actual lateral force.

3.1.1 Upper Level Controller

The objective of the upper level controller is to calculate the desired front lateral force, corresponding to road information and vehicle states. From the 2 DOF bicycle model in Figure 3.2, assuming a small steering angle, equations of motion are written as

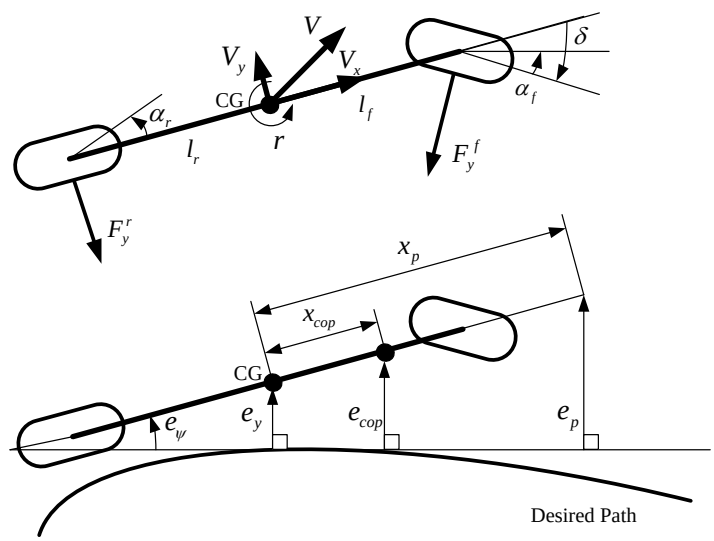

Figure 3.2 2 DOF bicycle model – defined vehicle parameter and errors

$$\begin{cases} F_y^f + F_y^r = m(\dot{v}_y + v_x r) \\ l_f F_y^f - l_r F_y^r = I_{zz}\dot{\gamma} \end{cases} \tag{3.1}$$

where F_y^f is the lateral force of the front wheel, m is the vehicle's mass, v_y is the lateral velocity, v_x is the longitudinal velocity, γ is the yaw rate, l_f and l_r are the vehicle parameters defined in Figure 3.2, and I_{zz} is the yaw moment of inertia.

The objective of developing a steering control system is to reduce error with respect to the desired road. Therefore, the state variables are transformed with lateral and yaw error in a dynamic model [16]. Errors are defined as

$$\begin{aligned} e_{\psi} &= \psi - \psi_{road} \\ e_{p} &= e_{y} + x_{p} \sin e_{\psi} \end{aligned} \tag{3.2}$$

where ψ is the yaw angle of the vehicle, ψ_{road} is the road heading angle, x_p is the projected distance and error terms are presented in Figure 2. Utilizing vehicle parameters and calculating, the second time derivative of errors is written as [15]

$$\begin{aligned} \ddot{e}_{\psi} &= \frac{l_f F_y^{\,f} - l_r F_y^{\,r}}{I_{zz}} - K\ddot{s} - \dot{K}\dot{s} \\ \ddot{e}_{p} &= \frac{F_y^{\,f} + F_y^{\,r}}{m} - V_x K\dot{s} + x_p\left(\frac{l_f F_y^{\,f} - l_r F_y^{\,r}}{I_{zz}} - K\ddot{s} - \dot{K}\dot{s}\right) \end{aligned} \tag{3.3}$$

where K is the path curvature and s is the travelled distance.

The feedforward part of the upper level controller is autonomous steering proposed by Kritayakirana and Gerdes [15]. In this paper, the method is used because the proposed method is well validated via experiments and can make dynamic equation simpler. The objective of the feedforward part is to eliminate the dynamics of the second time derivative of lateral error. $\ddot{e}_{cop}$ can be easily obtained by substituting x_{cop} in equation (3.3). x_{cop} is the distance between the center of gravity and center of percussion about the rear tyre and is written with vehicle parameters as

$$x_{cop} = \frac{I_{zz}}{ml_r} \tag{3.4}$$

From, equation (3.3) and (3.4),

$$\ddot{e}_{cop} = \frac{L}{l_r}\frac{F_y^{\,f}}{m} - v_x K\dot{s} - x_{cop}(K\ddot{s} + \dot{K}\dot{s}) \tag{3.5}$$

where L is the wheelbase of the vehicle. $F_y^{\,f}$, which can be controlled with

steering input is only remaining factor. From the objective of the feedforward part, the desired lateral front wheel force of the feedforward part is written as [15]

$$F_y^{FFW}(t) = \frac{ml_r}{L}(v_x(t)K\dot{s}(t) + x_{cop}(K\ddot{s}(t) + \dot{K}\dot{s}(t))) \tag{3.6}$$

Dividing the front tyre force input into F_y^{FFW} and F_y^{FB} parts ($F_y^f = F_y^{FFW} + F_y^{FB}$) and substituting F_y^{FFW} from equation (3.6) into (3.3) and (3.5), the equations of motion can, consequently, be written in state form as:

$$\frac{d}{dt}\begin{bmatrix} e_{cop} \\ \dot{e}_{cop} \\ e_\psi \\ \dot{e}_\psi \end{bmatrix} = \begin{bmatrix} 0 & 1 & 0 & 0 \\ 0 & 0 & 0 & 0 \\ 0 & 0 & 0 & 1 \\ 0 & 0 & 0 & 0 \end{bmatrix}\begin{bmatrix} e_{cop} \\ \dot{e}_{cop} \\ e_\psi \\ \dot{e}_\psi \end{bmatrix} + \begin{bmatrix} 0 \\ \frac{L}{ml_r} \\ 0 \\ \frac{l_f}{I_{zz}} \end{bmatrix} F_y^{FB} + \begin{bmatrix} 0 \\ 0 \\ 0 \\ -\frac{l_r}{I_{zz}} \end{bmatrix} F_y^r + \begin{bmatrix} 0 \\ 0 \\ 0 \\ \frac{v_x K\dot{s}}{L} - \frac{l_r}{L}(K\ddot{s} + \dot{K}\dot{s}) \end{bmatrix}$$

(3.7)

The last term is the disturbance from the road curvature that front wheel steering cannot eliminate, unless it has an independent control system to control the rear tyre [15]. To incorporate F_y^r and express equation (3.7) to a standard form, dimensionless parameter η proposed by Talvala *et al* [19] is used [15]. The parameter η has a value of one when the tyre state is in a perfect linear region and zero when the tyre state is at infinite slip angle. It describes the rear tyre force as

$$F_y^r = -\eta_r C_r \alpha_r \tag{3.8}$$

where C_r is the cornering stiffness of the rear tyre when the slip angle is zero, α_r is the slip angle of the rear tyre and η_r is the dimensionless parameter to capture the nonlinear behavior of the rear tyre. Substituting F_y^r from equation (3.8) into equation (3.7), the new equation of motion in state-space form can be found as

$$\frac{d}{dt}\begin{bmatrix} e_{cop} \\ \dot{e}_{cop} \\ e_{\psi} \\ \dot{e}_{\psi} \end{bmatrix} = A \cdot \begin{bmatrix} e_{cop} \\ \dot{e}_{cop} \\ e_{\psi} \\ \dot{e}_{\psi} \end{bmatrix} + B \cdot F_y^{FB}$$

$$= \begin{bmatrix} 0 & 1 & 0 & 0 \\ 0 & 0 & 0 & 0 \\ 0 & 0 & 0 & 1 \\ 0 & \frac{l_r \eta_r C_r}{I_{zz} V_x} & -\frac{l_r \eta_r C_r}{I_{zz}} & -\frac{(l_r + x_{cop}) l_r \eta_r C_r}{I_{zz} V_x} \end{bmatrix} \begin{bmatrix} e_{cop} \\ \dot{e}_{cop} \\ e_{\psi} \\ \dot{e}_{\psi} \end{bmatrix} + \begin{bmatrix} 0 \\ \frac{L}{m l_r} \\ 0 \\ \frac{l_f}{I_{zz}} \end{bmatrix} \cdot F_y^{FB} \tag{3.9}$$

Vehicle dynamics are represented as the standard form of state space in equation (3.9). Note that tyre uncertainties in the dynamics are effectively reduced and the state equation becomes simpler.

The objective of the feedback part of the upper level controller is to provide path tracking stability and eliminate path tracking error due to unmodelled error in equation (3.9). In this paper, a new concept of a full state feedback controller which is suitable for use at the limits of handling is presented.

The goal of feedback controllers in the previous research is to make lateral and heading error converge to zero [11-16] with respect to road. The error dynamics and their performance index can be written as

$$\frac{d}{dt}\begin{bmatrix} e_y \\ \dot{e}_y \\ e_{\psi} \\ \dot{e}_{\psi} \end{bmatrix} = F \cdot \begin{bmatrix} e_y \\ \dot{e}_y \\ e_{\psi} \\ \dot{e}_{\psi} \end{bmatrix} + G \cdot u \tag{3.10}$$

$$J_E = \int_0^{\infty} (\rho_1 {e_y}^2 + \rho_2 {\dot{e}_y}^2 + \rho_3 {e_{\psi}}^2 + \rho_4 {\dot{e}_{\psi}}^2 + r u^2) dt$$

where F is the system matrix, G is the input matrix of each error dynamics, u is a control input, such as steering wheel angle or desired front lateral force and $\rho_1, \rho_2, \rho_3, \rho_4, r$ are the weighting factors. They show good tracking performance in moderate handling. In contrast, at the limits of handling such as rally racing and F1 racing, body slip angle becomes bigger due to high lateral acceleration and professional driving techniques, such as trail braking [17]. The body slip angle on the paved road with passenger car ranges from 3 to 7 degrees and is significantly large compared to that of normal driving. Due to the large body slip angle, the

direction of the vehicle's instantaneous velocity, i.e., vehicle motion direction, and heading angle are different and this difference results in yaw angle error. Note that even in the case of a vehicle in a well tracking situation, as seen in Figure 3.3, the previous control law makes non-zero control input for regulating yaw error, the goal of the previous control law. In addition, when the controller eventually aligns vehicle heading angle with the road heading angle, lateral error due to non-zero lateral velocity occurs.

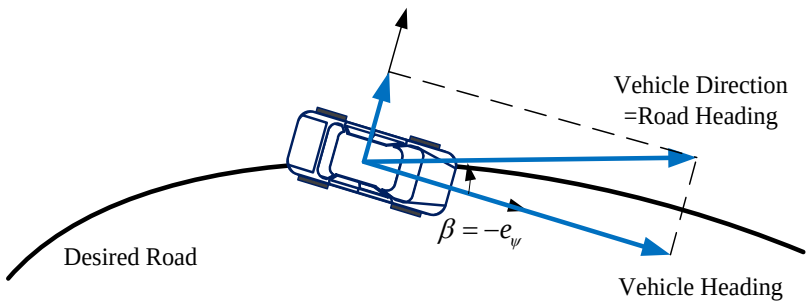

Figure 3.3. Well tracking situation : Yaw error occurring due to body slip angle

Furthermore, residual of lateral force and tyre damping, which can provide vehicle yaw stability, is very small because most of the tyre force is used for cornering and accelerating at the limits of handling. Therefore, in the case of existing feedback control law, the difference between vehicle direction and heading angle results in steering wheel angle oscillation and yaw error oscillation. This steering wheel angle oscillation makes the vehicle unstable, especially at the limits; thus, it is not desirable. Therefore, we should consider body slip angle in the feedback control law for good tracking performance and stability at the limits of handling.

Moreover, previous control laws which minimize yaw error do not mimic professional human drivers. Frequently, professional human drivers recognize and use unavoidable body slip angle and align vehicle direction with road heading angle, i.e., zero tangential error, not vehicle heading angle with road heading angle in cornering. Therefore, steering wheel angle oscillation does not occur in the real situation. Professional human drivers do not manipulate steering wheel angle in a low frequency and they are invited to keep steering movement to a minimum [18]. To reflect these aspects, the role of the feedback controller which minimizes yaw error should be replaced with minimizing the sum of body slip angle and yaw error, i.e., the controller makes vehicle direction align with the desired road heading angle for zero tangential error. When the vehicle is driven on a straight road, body

slip angle goes to zero, and the sum of body slip angle and yaw error becomes yaw error as the previous feedback controller.

The basic control law of the new feedback controller at the limits of handling is to minimize the performance index which is written as:

$$J_P = \int_0^\infty (\rho_1 e_y{}^2 + \rho_2 (e_\psi + \beta)^2 + \rho_3 (\dot{e}_\psi)^2 + r F_{FB}{}^2) dt \tag{3.11}$$

The objective of the control law is to minimize lateral error with e_y and tangential error with $e_\psi + \beta$ which represents the difference between vehicle direction and road heading angle as seen in Figure 3.4. This error should be minimized to keep the vehicle on the desired path, and match the vehicle motion direction and road direction. However, although lateral and tangential errors converge to zero, yaw error can oscillate because there is no constraint of yaw error. Therefore, yaw damping is added for reducing yaw error with adding $\dot{e}_\psi$ in the performance index. To obtain gain set of the feedback controller, body slip angle should be expressed in terms of vehicle error states in equation (3.9).

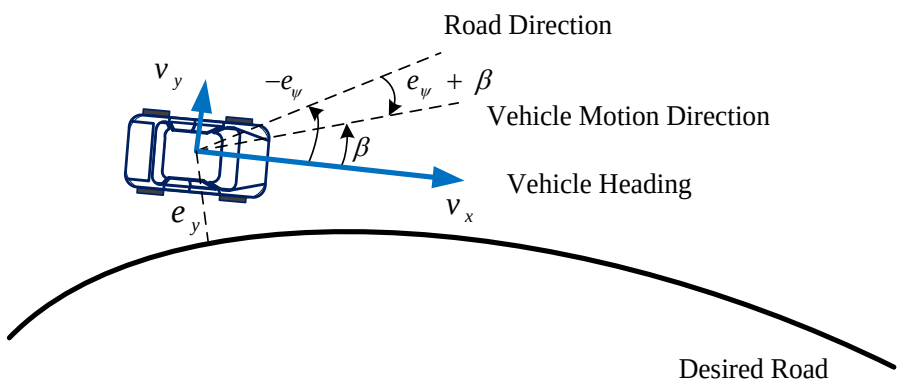

Figure 3.4. Feedback controller at the limits of handling

The time derivative of lateral error $\dot{e}_y$ is written as

$$\begin{aligned}\dot{e}_y &= v_x \sin e_\psi + v_y \cos e_\psi \\ &= v_x \sin e_\psi + v_x \tan\beta \cos e_\psi \quad \left(\because \tan\beta = \frac{v_y}{v_x} \right)\end{aligned} \tag{3.12}$$

Multiplying $\cos\beta$ and applying the sin of sum identity, the new equation is written as

$$e_\psi + \beta = \sin(e_\psi + \beta) = \frac{\dot{e}_y}{v_x}\cos\beta = \frac{\dot{e}_y}{v} \tag{3.13}$$

The small angle approximation about $e_\psi + \beta$ in equation (3.13) is reasonable because the objective of the feedback controller is to eliminate tangential error $e_\psi + \beta$. Because the tangential error $e_\psi + \beta$ is expressed in terms of $\dot{e}_y$, the performance index is re-written as

$$J = \int_0^\infty (\rho_1 {e_y}^2 + \frac{\rho_2}{V^2}{\dot{e}_y}^2 + \rho_3(\dot{e}_\psi)^2 + r{F_{FB}}^2)dt \tag{3.14}$$

where ρ_1, ρ_2, ρ_3 is the weighting factors which corresponds to each error. The equation consists of lateral error e_y and time derivative of lateral error $\dot{e}_y$, not e_{cop} and $\dot{e}_{cop}$ as equation (3.9). Therefore, e_{cop} and $\dot{e}_{cop}$ should be transformed into e_y and $\dot{e}_y$ by using equation (3.2). Its transformation matrix is written as

$$\begin{bmatrix} e_{cop} \\ \dot{e}_{cop} \\ e_\psi \\ \dot{e}_\psi \end{bmatrix} = \begin{bmatrix} 1 & 0 & x_{cop} & 0 \\ 0 & 1 & 0 & x_{cop} \\ 0 & 0 & 1 & 0 \\ 0 & 0 & 0 & 1 \end{bmatrix} \cdot \begin{bmatrix} e_y \\ \dot{e}_y \\ \sin e_\psi \\ \cos e_\psi \cdot \dot{e}_\psi \end{bmatrix} = \begin{bmatrix} 1 & 0 & x_{cop} & 0 \\ 0 & 1 & 0 & x_{cop} \\ 0 & 0 & 1 & 0 \\ 0 & 0 & 0 & 1 \end{bmatrix} \cdot \begin{bmatrix} e_y \\ \dot{e}_y \\ e_\psi \\ \dot{e}_\psi \end{bmatrix} \tag{3.15}$$

In equation (3.15), small angle assumption of e_ψ is used for linearization. Substituting errors in equation (3.9) from equation (3.15), the new equation of motion is written in terms of lateral error and yaw error as,

$$\frac{de}{dt} = T^{-1}ATe + T^{-1}BF_{FB} = \mathrm{A}_z\mathrm{e} + \mathrm{B}_z F_{FB}$$

$$\text{where } e = \begin{bmatrix} e_y \\ \dot{e}_y \\ e_\psi \\ \dot{e}_\psi \end{bmatrix}, T = \begin{bmatrix} 1 & 0 & x_{cop} & 0 \\ 0 & 1 & 0 & x_{cop} \\ 0 & 0 & 1 & 0 \\ 0 & 0 & 0 & 1 \end{bmatrix}, A_z = T^{-1}AT,\ B_z = T^{-1}B \tag{3.16}$$

where T is the transformation matrix in the equation (3.15), A is the system matrix, B is the input matrix in the state space equation (3.9), A_z is the new system matrix and B_z is the new input matrix in the state space equation (3.16).

The goal of the feedback controller is to minimize the performance index given in equation (3.17).

$$J = \int_0^\infty (e^T Qe + u^T Ru)dt$$

$$\text{where } Q = \begin{bmatrix} \rho_1 & 0 & 0 & 0 \\ 0 & \dfrac{\rho_2}{V^2} & 0 & 0 \\ 0 & 0 & 0 & 0 \\ 0 & 0 & 0 & \rho_3 \end{bmatrix},\ R = r,\ u = F_y^{FB} \tag{3.17}$$

Because the magnitude of the control input is not important at the limits of handling, r is chosen as a small value. ρ_1, ρ_2, ρ_3 are the weighting factors which correspond to each error. To follow the desired road, both lateral error and tangential error are important; especially, tangential error is more important at the limits of handling to stabilize the vehicle. Therefore, the weighting factor of tangential error ρ_2 is set as a large value. Furthermore, even if we minimize the tangential error, the yaw error can oscillate because there is no constraint in the yaw angle direction. Therefore, the weighting factor of yaw damping ρ_3 is set to eliminate yaw error oscillation. To satisfy the above requirements, consequently the weighting factors are determined as $\rho_1 = 50$, $\rho_2 = 2000$, $\rho_3 = 300$, and $r = 0.000001$. Because there is velocity V is in the weighting matrix Q, gain scheduling with respect to V is conducted before on-line simulation.

Using linear quadratic optimal control theory, feedback input is solved as [20]

$$0 = -A_z^T H_{ss} - H_{ss} A_z + H_{ss} B_z R^{-1} B_z^T H_{ss} - Q$$
$$F_y^{FB} = -K_g \cdot e = -R^{-1} B_z^T H_{ss} \cdot e \tag{3.18}$$

where K_g is the gain and H_{ss} is the solution of the Riccati equation. Feedback control input is full-state feedback. Because the state equation is simplified by the benefits of using COP, the selection of weighting factor and variables is not complicated.

Even though LQR is robust and its stability is already proved, it does not guarantee stability of closed-loop system due to model uncertainty and actuator limitation. However, in this paper actuator limitation is not considered.① As seen in equations (3.7) and (3.9), dynamic equation is force-based equation and all of nonlinear tire dynamics is considered with parameter η_r. Moreover, disturbance vector consists of bounded variables such as longitudinal speed and curvature. Thus, model uncertainty and disturbance vector are bounded and do not affect to stability② [15]. To check stability of control system, Lyapunov theory is used. If a matrix P meets under conditions, the closed-loop dynamics $\dot{x} = A_{CL} x$ is stable.

for all nonzero z
$$V_{lyap} = z^T P z > 0$$
$$\dot{V}_{lyap} = z^T (A_{CL}^T P + P A_{CL}) z < 0 \tag{3.19}$$

By use of linear matrix inequality solver (http://kr.mathworks.com/help/robust/ref/feasp.html), P can be easily founded [15]. Due to scheduled gain with respect to vehicle velocity, η_r is the only variable. In this paper, η_r is in $0.28 \le \eta_r \le 1$. From Talvala *et al* [19], $\eta_r = 0.28$ means saturated situation and $\eta_r = 1$ means perfectly elastic region of tyre.

$$A_{CL,\eta_r=0.28}^T P + P A_{CL,\eta_r=0.28} < 0$$
$$A_{CL,\eta_r=1}^T P + P A_{CL,\eta_r=1} < 0 \tag{3.20}$$
$$where\ A_{CL,\eta_r=\xi} = A\big|_{\eta_r=\xi} - B \cdot K$$

① As seen in overall simulations, steering wheel angle did not exceed 200 deg where the maximum angle is 720 deg. Because the algorithm is focused on limit handling of vehicle, there is no case to use maximum steering angle.

② Appropriate gain set can regulate bounded uncertainty.

All of results show that the control system is stable in the sense of Lyapunov. For example, when longitudinal speed is 20m/s, a P can be solved as

$$P = 10^4 \cdot \begin{bmatrix} 0.0104 & 0.0022 & 0.0339 & -0.0040 \\ 0.0022 & 0.0064 & 0.0038 & -0.0110 \\ 0.0339 & 0.0038 & 1.2521 & 0.0126 \\ -0.0040 & -0.0110 & 0.0126 & 0.0501 \end{bmatrix} \tag{3.21}$$

As a result, the LQR gain can stabilise the plant from moderate ($\eta_r = 1$) to limit ($\eta_r = 0.28$) maneuvering.

Consequently, the overall upper level control input is the sum of feedforward and feedback control input as seen in equation (3.22).

$$\begin{aligned} F_y^{\,f}(t) &= F_y^{FFW}(t) + F_y^{FB}(t) \\ &= \frac{ml_r}{L}\left(V_x(t)K\dot{s}(t) + x_{cop}(K\ddot{s}(t) + \dot{K}\dot{s}(t))\right) - R^{-1}B_z{}^T H_{ss} \cdot \begin{bmatrix} e_y \\ \dot{e}_y \\ e_\psi \\ \dot{e}_\psi \end{bmatrix} \end{aligned} \tag{3.22}$$

Feedforward and feedback control inputs are coupled and provide a general outline of the desired lateral force and path tracking stability, respectively.

3.1.2 Lower Level Controller

The objective of the lower level controller is to convert the front lateral force to steering wheel angle input. Because upper level controller is designed by forced-based approach, the control command of the upper level controller is front lateral force. However, the lateral motion of vehicle is manipulated with steering wheel angle. Therefore, conversion of the front lateral force to steering wheel angle should be conducted. This paper presents an effective conversion by utilizing the 2 DOF bicycle model and calculation of the understeer gradient based on theory of self-tuning controller with bounded-gain-forgetting (BGF) estimator.

The objective of the feedforward part of the lower level controller is to provide the nominal steering wheel angle which corresponds to front lateral force. The input is designed with the 2 DOF bicycle model. From the geometry of 2 DOF

model, steering angle is represented in terms of wheel base L, slip angles α_f and α_r, and road radius R, as seen in equation (3.23)[16].

$$\delta = \frac{L}{R} + \alpha_f - \alpha_r \tag{3.23}$$

The slip angles in equation (3.23) can be written in terms of understeer gradient K_{us} as

$$\delta = \frac{L}{R} + K_{us} a_y$$
$$\text{where } K_{us} = \frac{W_f}{C_f} - \frac{W_r}{C_r} \tag{3.24}$$

As seen in equation (3.24), road radius R and understeer gradient K_{us} should be represented in terms of the vehicle parameters and the control command to calculate steering control input which corresponds to the desired lateral tyre force. First, road radius can be easily obtained from the equation of motion of the vehicle. Assuming that the vehicle is on steady-state cornering, equations of motion from equation (3.1) are written as,

$$\begin{cases} F_y^f + F_y^r = \dfrac{m v_x^{\,2}}{R} \\ l_f F_y^f - l_r F_y^r = 0 \end{cases} \tag{3.25}$$

From equation (3.25), road curvature K is written as,

$$K = \frac{1}{R} = \frac{1}{m v_x^{\,2}} \cdot \frac{L}{l_r} \cdot F_{y,des}^f \tag{3.26}$$

where $F_{y,des}^f$ is the desired front lateral force which is the control input of the upper level controller. Second, understeer gradient K_{us} can be calculated from estimation of cornering stiffness as the definition. However, there is not a simple, satisfactory estimation of cornering stiffness. Therefore, a parameter adaptation approach is chosen in this paper. Adaptive control is to estimate the uncertain

parameter and use the estimated parameter in control input [20]. Bounded-Gain-Forgetting estimator is kinds of least-squares estimator which minimizes the total prediction error, time integral of error. However, the total prediction error contains past error data which are generated from the past parameter and disturbs tracking varied parameter. Because understeer gradient, the parameter to be estimated, is time-varying, simple least-squares estimator is not suitable and the past data should be forgotten. Thus, authors applied self-tuning adaptive controller with BGF estimator. To apply the theory, adaptation law should be formulated as linear parameterization model as seen in equation (3.27)

$$\delta - \frac{L}{R} = \hat{K}_{us} a_y \tag{3.27}$$

Using the theory of BGF estimator, understeer gradient can be solved as seen in equation (3.28) [20],

$$\begin{aligned} &\hat{K}_{us} = -P(t) a_y e_1(t) \\ &e_1 = (\delta - \frac{L}{R}) - \hat{K}_{us} a_y \\ &\frac{d}{dt}[P(t)] = P(t)\lambda(t) - P(t)^2 a_y^2 \\ &\lambda(t) = \lambda_0 (1 - \frac{|P|}{k_0}) \end{aligned} \tag{3.28}$$

where k_0 and λ_0 is tuning parameter which related to convergence speed and forgetting constant respectively. A gain set of BGF estimator is $k_0 = 10$ and $\lambda_0 = 3$. This algorithm is well tracked the time-varying parameter and its convergence is mathematically proved. [20] Moreover, because the theory BGF estimator is based on minimizing the following cost function, it is robust to measurement noise.

$$\begin{aligned} &J = \int_0^t \exp[-\int_s^t \lambda(r) dr] \{z(s) - \hat{K}_{us} a_y(s)\}^2 ds \\ &\text{where } z = \delta - \frac{L}{R} \end{aligned} \tag{3.29}$$

Substituting road radius from equation (3.26), the feedforward steering angle

relationship is written as

$$\delta_{FFW}(t) = \frac{L^2}{l_r} \cdot \frac{F_{y,des}^{f}(t)}{mV_x(t)^2} + \hat{K}_{us}(t)a_y(t) \tag{3.30}$$

where understeer gradient K_{us} can be obtained from equation (3.27). Note that the feedforward steering angle relationship, equation (3.30), is only represented in terms of vehicle parameter and control input of upper level controller, front lateral tyre force, without estimation of tire parameter. Consequently, given upper level control command $F_{y,des}^{f}$, feedforward steering input corresponding to the desired front lateral tyre force can be easily obtained from the vehicle parameter.

The objective of the feedback part of the lower level controller is to compensate for uncertainty and unmodelled error of the feedforward part. Moreover, for the purpose of fast adaptation convergence, feedback part is essential. The feedback part is designed by a simple PI controller with respect to front lateral tyre force error, i.e., the difference between the desired lateral force and measured lateral force, because the difference between the feedforward steering angle and the desired steering angle. A gain set can be easily obtained by trial and error. This can be replaced with the difference with respect to the related parameter.

$$\delta_{FB}(t) = K_P \cdot \Delta F_y^{f}(t) + K_I \cdot \int \Delta F_y^{f}(t)dt \tag{3.31}$$

where K_P is the proportional gain, K_I is the integral gain and ΔF_y^{f} is the lateral force error. A gain set of feedback controller is $K_P = 0.019$ and $K_I = 0.043$. Because this paper is focused on driver model for closed loop simulation, actual lateral force is used to calculate the lateral force error in the feedback algorithm. Consequently, conversion of the desired front lateral tyre force to desired steering wheel angle is achieved as equation (3.32).

$$\begin{aligned}\delta(t) &= \delta_{FFW}(t) + \delta_{FB}(t) \\ &= \frac{L}{l_r} \cdot \frac{F_{y,des}^{f}(t)}{mV_x(t)^2} \cdot (L + \frac{K_{us}(t) \cdot V_x(t)^2}{g}) + K_P \cdot \Delta F_y^{f}(t) + K_I \cdot \int \Delta F_y^{f}(t)dt\end{aligned} \tag{3.32}$$

The feedforward part of the lower level controller provides nominal steering input which corresponds to upper level control input and the feedback part of the lower level controller compensates for unmodelled error.

Because the proposed algorithm that consists of upper and lower level controller is only based on PI controller and kinematic variables such as travelled distance, vehicle speed, vehicle parameter and etc., nonlinear characteristics of tire model due to combined slip is inherently considered. As tires confront combined slip, the characteristics of vehicle motion changes and this varied characteristics is reflected in the proposed algorithm.

3.2. Comparison and Validation

All of the simulations for evaluation of lateral driver model are performed with Matlab Simulink and Carsim.③. In Section 3.2.1, the proposed feedback control law is compared with the existing feedback control law on an ideal road. In Section 3.2.2, the proposed lower level control algorithm is validated on an ideal road with respect to various road friction coefficients. In Section 3.2.3, the same comparison is conducted on a complex corner in the Korea International Circuit (KIC). In addition, through using driver data, results of the proposed and existing feedback control laws are compared with driver data. In Section 3.2.4, comparison of the proposed model with the driver data and the existing preview model is conducted to validate tracking performance and similarity with professional drivers. Vehicle parameters of Carsim F class have been modified to obtain similar dynamic characteristics of the test vehicle.

3.2.1. Comparison of the Proposed with the Existing Feedback Control Law on an "S" Shape Road

In this section, comparison of the proposed feedback control law with existing feedback control law is conducted in an ideal condition. The existing feedback which is used in this section for comparison is presented by Kritayakirana and Gerdes[15]. It is based on the lane-keeping system proposed by Rossetter *et al* [21]. It has sufficient yaw damping to compensate for yaw oscillation and its stability is investigated via Lyapunov theory. The proposed feedback control which minimizes tangential error has been presented in the previous section. The main difference between the existing and the proposed feedback control law is whether body slip angle is considered. The simulation is performed in the condition in which lateral acceleration is 0.96g and an "S" shape corner which consists of clothoid and circle as Lopez[22] when $\mu = 1$. Simulation results are presented in Figure 5 and Figure 6. The existing feedback controller is presented as "w/o Beta considered" and the proposed controller is presented as "w/ Beta considered" in the legend of the graphs.

Even though the existing feedback has sufficient yaw damping, steering wheel angle oscillation and yaw error oscillation occurred. Moreover, this phenomenon is occurred near the friction limits as seen in Figure 3.5, which shows this phenomenon is not occurred below the friction limits (lateral acceleration is 0.82g). As described in the previous section, steering wheel angle oscillation results in instability of the vehicle and does not mimic the professional driver, who

③ Sampling time : 0.01 sec

is invited to keep steering movement to a minimum [18]. However, the proposed feedback controller which considers body slip angle eliminates steering angle oscillation. In addition, oscillation of body slip angle and yaw error is eliminated as seen in Figure 3.6. In addition, steering angle and yaw error oscillation is also shown while friction coefficient is varied as seen in Figure 3.7.

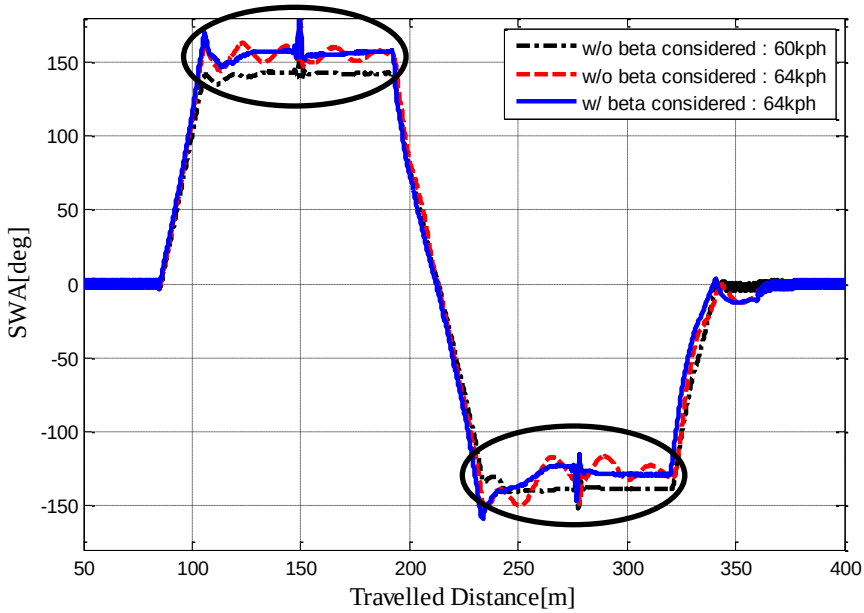

Figure 3.5. Steering wheel angle comparison

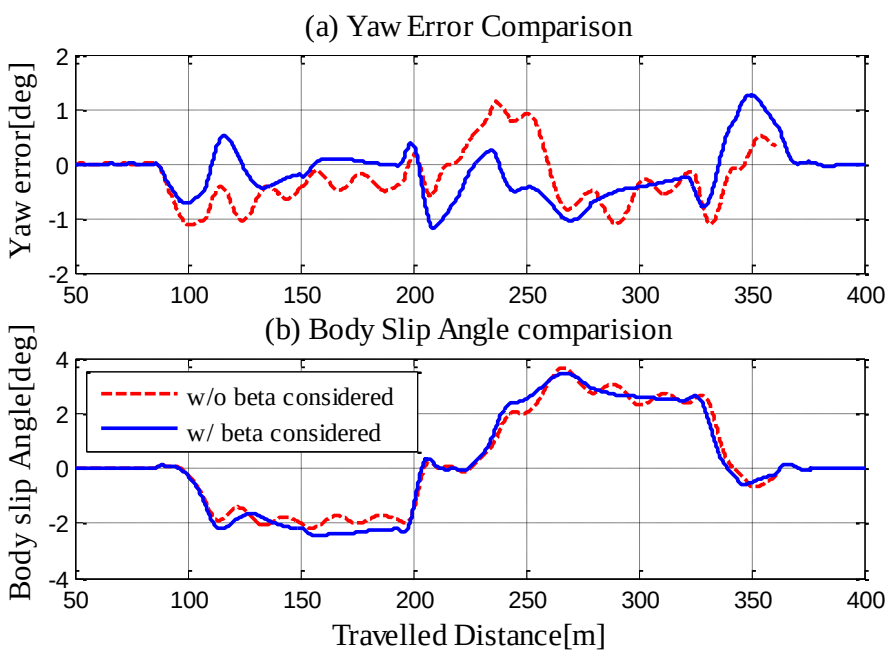

Figure 3.6. Yaw error and Body slip angle comparison

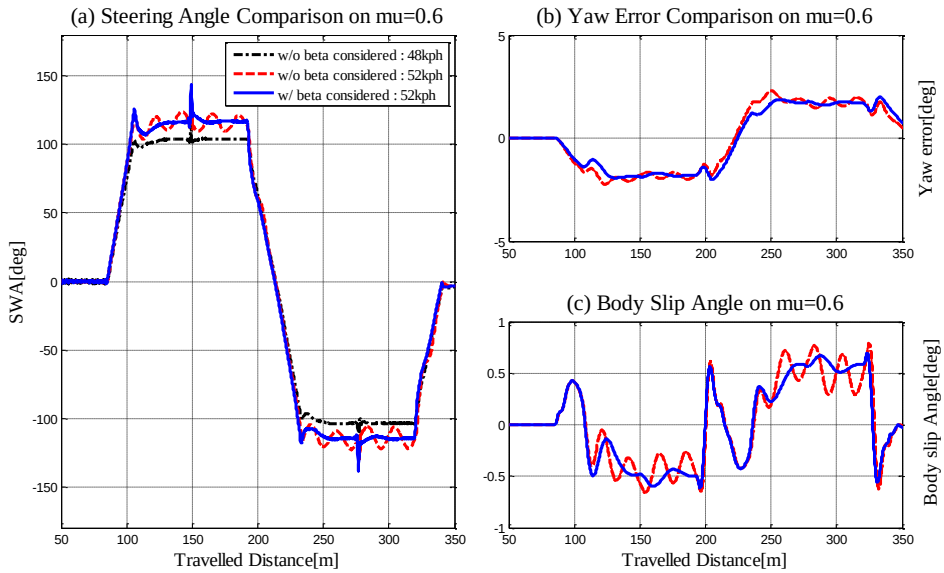

Figure 7. Simulation Results of Wet Road Condition

Because l_f and l_r of the vehicle model are similar in size, i.e. $l_f \approx l_r$, the body slip angle is small. However, in many cases, due to many reasons such as saturated rear tyre, the vehicle easily becomes unstable; this results in large body slip angle, especially at the limits of handling. Moreover, professional drivers sometimes intend to make side slip angle such as trail braking [17]. In addition, in the case of small body slip angle, tangential error converges to yaw error. Therefore, tangential error is a generalized form of yaw error.

3.2.2 Validation of the Proposed Lower Level Control Algorithm on the "S" Shape Road

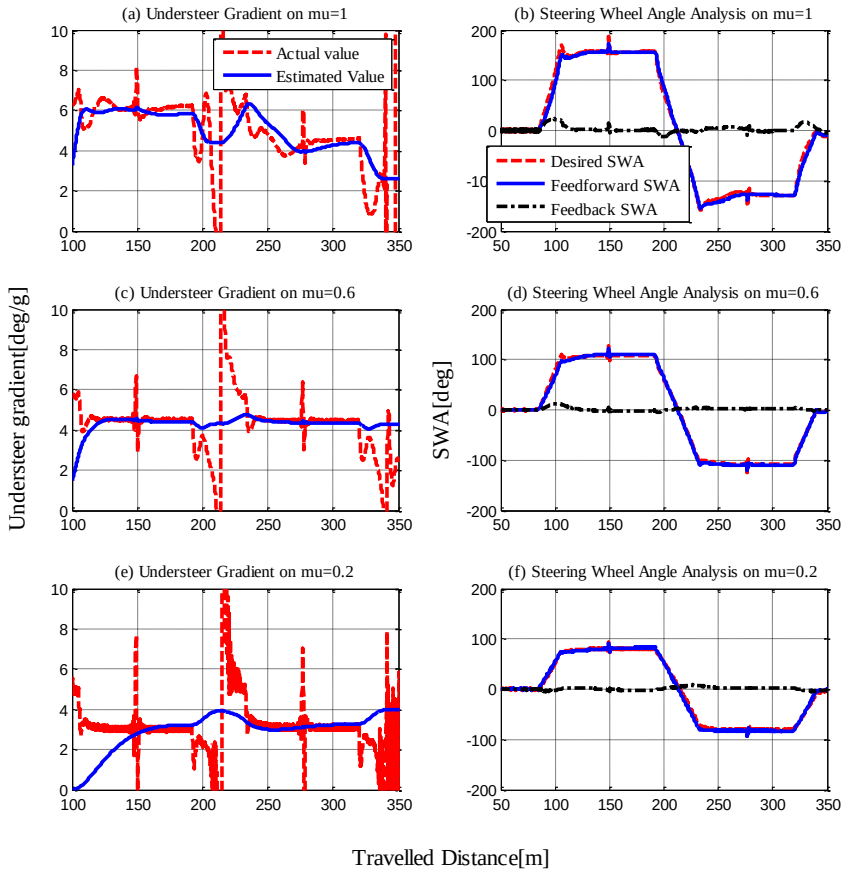

Figure 3.8. Performance of Lower Level Algorithm

In this section, validation of the proposed lower level control algorithm is conducted on the "S" shape road with respect to various friction coefficients. The simulation is performed in the condition in which lateral acceleration is over $0.9\,\mu$ g with the proposed lateral driver model. Friction coefficients are set as $\mu = 1, 0.6, 0.2$ which represent dry, wet, and snowy road condition respectively.

The simulation results are presented in Figure 3.8. Plots of understeer gradient, adaptive parameter, and comparison of desired, feedforward, and feedback steering wheel angle in each friction coefficient is shown. Actual value of understeer gradient is from Carsim output.

Even though convergence speed of adaptive parameter becomes slow as friction coefficient decreased and actual understeer gradient is oscillated, estimated value

well tracks the trend value of actual value. Root mean square value of difference between desired steering wheel angle and feedforward steering wheel angle is calculated as 6.18deg (4.1% of maximum steering angle), 2.87deg (2.4% of maximum steering angle), and 2.59deg (3.0% of maximum steering angle) with respect to each friction coefficient respectively. Note that the feedforward steering wheel angle has similar value with desired steering wheel angle. Because the proposed algorithm, driver model, is focused on closed loop simulation, for the purpose of accuracy, the actual lateral force is used to calculate force error.

3.2.3 Comparison of the Proposed with the Existing Feedback Control Law on Korea Interntional Circuit

In this section, the same comparison of Section 3.2.1 is conducted on a complex corner in the Korea International Circuit. Moreover, driver experiment data are added in a comparison target for reference. The driver data are acquired from the Korea International Circuit with luxury sedan weighting 2000 kg. To validate tracking performance and similarity with human drivers of the proposed lateral driver model, three consecutive corners which are to evaluate the controller's ability to react to the various corners are selected in the track. The radius of each corner is 25m, 20m and 18m, respectively, and the corners are a flat, paved road. Note that, at the limits of handling, there are not many styles of steering behaviour with respect to drivers such as moderate maneuver because vehicle is on the boundary of stability. Furthermore, professional drivers are invited to keep the optimal line for each lap. Therefore, single driver data from a professional driver are used.

Because the proposed driver model is limited to the lateral driver model, the desired path and velocity profile are obtained from driver data which are generated by RT 3000. It is often to consider longitudinal and lateral control independent on previous researches [15, 23]. Thus, the longitudinal part to follow the desired speed independently combined to the proposed algorithm. To calculate more reliable error and curvature, the desired path should be smoothed. Smoothing algorithm is conducted through optimizing cost function in equation (3.33) which is proposed by Thrun *et al* [23].

$$\underset{x_1,\cdots,x_n}{\operatorname{argmin}}\left[\sum_i \left(y_i - x_i\right)^2 - \sum_n W_{cur}\frac{\left(x_{n+1}-x_n\right)\cdot\left(x_n-x_{n-1}\right)}{|\,x_{n+1}-x_n\,||\,x_n-x_{n-1}\,|}\right] \tag{3.33}$$

where y_i is the original trajectory, W_{cur} is the weighting parameter and x_i is

the smoothed path. The first term of the cost function presents the distance between the original trajectory and smoothed path. The second term presents the cosine value of the included angle between adjacent vectors and minimizes curvature. After smoothing the trajectory, discrete points are connected through natural cubic splines [24].

The simulation results are presented in Figure 3.10, and Figure 3.11. Figure 3.9 is the overall curvature of the desired path, and Figure 3.10 is a comparison of the steering wheel angle.

It is hard to find advantages of the proposed feedback control law in Figure 3.10. In addition, there is no steering wheel angle oscillation because the vehicle is not strictly at the boundary of the stability and the given track does not have constant curvature as the previous “S” shape corner. However, in Figure 3.11 which show lateral error with respect to the driver data, respectively, the advantage of the proposed feedback control law can be found. As seen in Figure 3.11, the maximum value of lateral error becomes large with negotiating the consecutive corner. When the driver negotiates the consecutive corner at the limits of handling, the driver always confronts the next corners with unstable vehicle states such as non-zero body slip angle and roll angle. However, professional drivers do not recognize non-zero body slip angle as yaw error as the existing control law, because their ultimate goal is to track the desired optimal path not stabilizing the vehicle. Moreover, the existing feedback control law recognizes body slip angle as yaw error and tries to reduce it. Consequently, unnecessary tyre force is needed to stabilize the vehicle in the yaw direction.

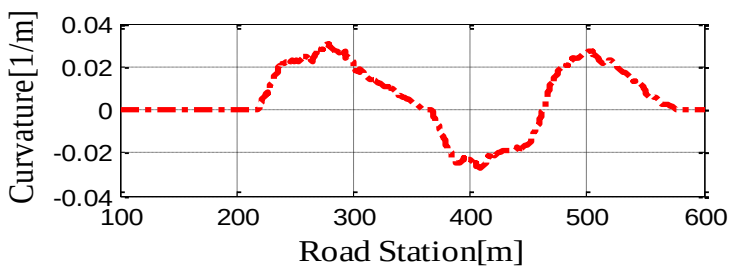

Figure 3.9. Overall curvature with respect to road station

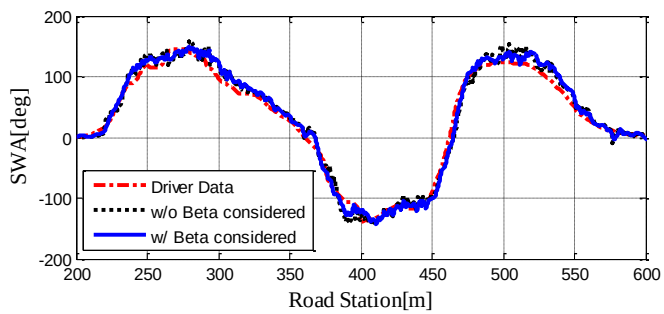

Figure 3.10. Comparison : steering wheel angle

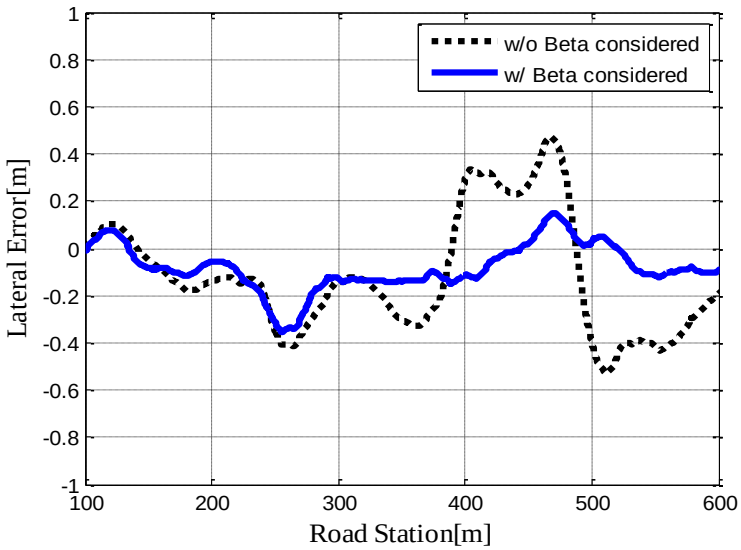

Figure 3.11. Comparison : lateral error w.r.t. driver data

As shown in Figure 3.9 and Figure 3.11, both feedback control laws show similar tracking performance on the first corner (200m~360m in the road station). However, as the vehicle goes through the second corner(360m~460m in the road station) and the third corner(460m~580m in the road station), it becomes unstable, and the existing feedback controller presents worse tracking performance than the proposed feedback controller because it tries to stabilize the vehicle as seen in Figure 3.11. From the above results and discussion, the proposed feedback control law shows better tracking performance than the existing feedback control law at the limits of handling.

3.2.4 Comparison of the Driver Models

In this section, the proposed lateral driver model is compared with the human driver data and the existing preview steering controller. The driver data are acquired in the Korea International Circuit (KIC) with luxury sedan weighting 2000 kg. The preview driver model which is proposed by Kang *et al* [25] is designed based on the optimal finite preview method with respect to the 2 DOF bicycle model, and it consists of a feedforward and feedback part. The gain of the feedback part is well tuned to minimize lateral error and assure yaw stability.

The simulation result is shown in Figure 3.12, Figure 3.13, and Figure 3.14. In Figure 3.12, lateral error with respect to driver data is presented. In a quantitative respect, lateral error is bounded above by 0.2m and below by -0.4m, even though

the simulated vehicle is at high lateral acceleration. In contrast, lateral error of the preview model ranges from -1m to 2m. In addition, it shows large lateral error which is due to instability of the vehicle between 380m~430m by the road station.

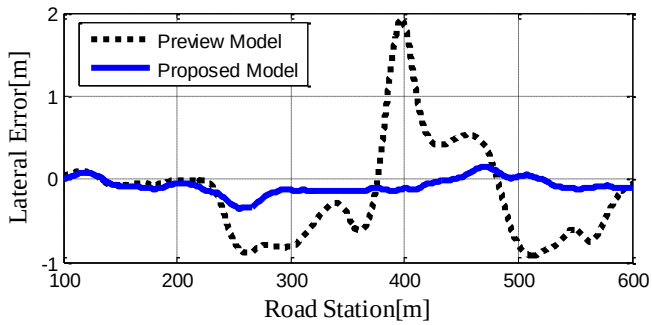

Figure 3.12. Simulation Result : lateral error w.r.t. driver data

Similarity with human drivers is investigated through comparison of steering wheel angle and body slip angle. The aspect of the steering wheel angle of the simulation result is similar to that of driver data, as seen in Figure 3.13. When the differences between the vehicle model in Carsim and the luxury sedan are taken into consideration, the steering angle difference is very small. Furthermore, the body slip angle shows similarity to human driver data, as seen in Figure 3.14. The body slip angle of the lateral driver model has similar magnitude and tendency to that of driver data.

In a quantitative respect, the standard deviation of the steering wheel angle and body slip angle difference is presented as seen in Table. 3.1. The proposed lateral driver model has more similar control input to human drivers than preview model. Also, this tendency is able to see in the case of body slip angle. The proposed lateral driver model shows more similar behaviour to human drivers than the preview model.

Table. 3.1. SWA and Body slip angle difference with respect to driver data

SWA Difference	Proposed Model	Preview Model
RMS Value	10.49(deg)	20.75(deg)
Beta Difference	Proposed Model	Preview Model
RMS Value	0.4394(deg)	0.9893(deg)

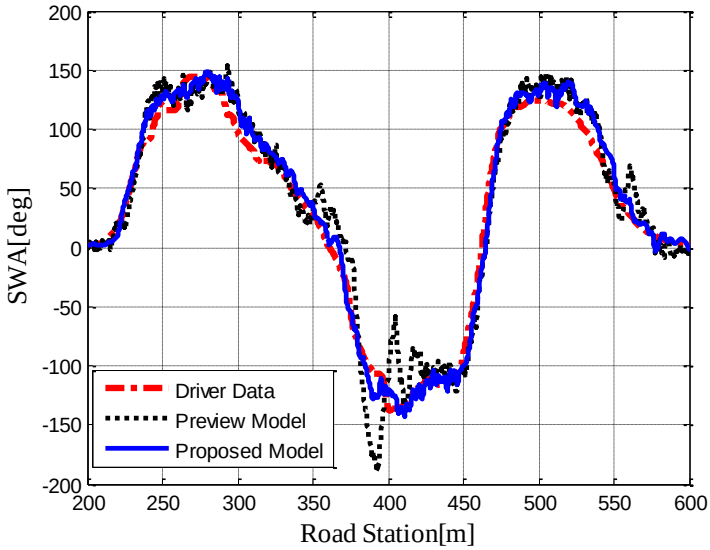

Figure 3.13. Comparison : steering wheel angle

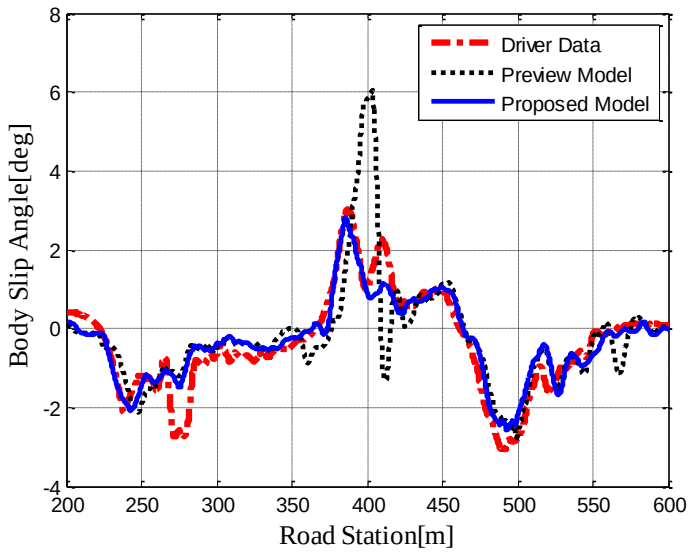

Figure 3.14. Comparison : body slip angle

From the above results, the proposed lateral driver model shows not only better performance but also more similar vehicle steering behaviour to human drivers, than the existing preview model.

Chapter 4

Development of Integrated Chassis Control Algorithm of ESC and 4WD for Enhanced Limit Handling

The block diagram of the control algorithm proposed in this study is shown in Fig. 4.1. The proposed algorithm consists of three layers. First, to interpret the driver intended motion, a supervisor determines the desired yaw rate and longitudinal acceleration based on the driver's commands and vehicle states. Second, to track the desired vehicle motion, an upper level controller determines the virtual control inputs, such as the desired longitudinal force and the desired yaw moment. Finally, based on virtual control inputs and vehicle states, a lower level controller optimally allocates actual control input to 4WD and ESC actuators.

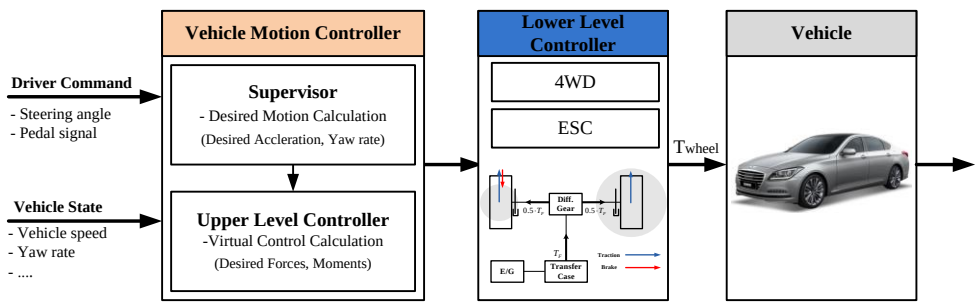

Figure 4.1. Block diagram of the control algorithm

4.1 Supervisor

The objective of the supervisor is to interpret the driver intended motion based on the driver's command and vehicle state. The desired yaw rate is designed with the 2DOF bicycle model. From the cornering kinematics of the bicycle model, the wheel steering angle can be written as [16]:

$$\delta = \frac{L}{R} + \alpha_f - \alpha_r \tag{4.1}$$

where δ is the wheel steering angle; L is the wheelbase; R is the road curvature; and α_i is the slip angle of each tire. The difference between the front

and rear slip angles in equation (4.1) can be re-written in terms of understeer gradient K_{us}, and road curvature R can be re-written by using the kinematic relation between the yaw rate and the velocity of the vehicle as [16]:

$$\delta = \frac{L\gamma}{v_x} + K_{us} a_y \tag{4.2}$$

where γ is the yaw rate; v_x is the longitudinal velocity; and a_y is the lateral acceleration of the vehicle. From equation (4.2), a desired yaw rate is designed as:

$$\gamma_{des} = \frac{v_x}{L} \cdot (\delta - K_{us} a_y) \tag{4.3}$$

where γ_{des} is the desired yaw rate. In this paper, because the algorithm is focused on limit handling, the desired understeer gradient is set to be zero for agile vehicle cornering maneuver. In other words, the vehicle tends to behave as neutral steer.

The desired longitudinal acceleration is determined based on the driver's pedal signal, which indicates the amount to accelerate. From the pedal signal, the desired longitudinal acceleration is determined by the use of a torque map and engine speed as [8]:

$$\begin{aligned} a_{x,driver} &= a_x(APS) + a_x(BPS) \\ v_{x,des}(k+1) &\approx v_x(k) + a_{x,driver} \cdot T_{sampling} \end{aligned} \tag{4.4}$$

here APS and BPS are the accelerator and brake pedal signal, respectively; and $v_{x,des}$ is the desired longitudinal velocity.

4.2 Uppel Level Controller

The objective of the upper level controller is to determine the desired yaw moment and desired longitudinal force to track the desired motion. Due to uncertainties of model uncertainties and disturbances, the desired longitudinal force and yaw moment are determined by the use of sliding mode control theory. This scheme is previously presented in [7-9].

4.2.1 Yaw Rate Controller

The objective of the yaw rate controller is to reduce the yaw rate error between the actual yaw rate and the desired yaw rate, which is determined by the supervisor. The yaw rate controller is designed with the re-arranged dynamic equation of the bicycle model. The equation of motion of the 2DOF bicycle model is described as [16]:

$$\begin{bmatrix}\dot{\beta}\\ \dot{\gamma}\end{bmatrix}=\begin{bmatrix}-\frac{2(C_f+C_r)}{m\cdot v_x} & -1-\frac{2(l_f\cdot C_f-l_r\cdot C_r)}{m\cdot {v_x}^2}\\ -\frac{2(l_f\cdot C_f-l_r\cdot C_r)}{I_z} & -\frac{2({l_f}^2\cdot C_f+{l_r}^2\cdot C_r)}{I_z\cdot v_x}\end{bmatrix}\cdot\begin{bmatrix}\beta\\ \gamma\end{bmatrix}+\begin{bmatrix}\frac{2\cdot C_f}{mv_x}\\ \frac{2\cdot l_f\cdot C_f}{I_z}\end{bmatrix}\cdot\delta+\begin{bmatrix}0\\ \frac{1}{I_z}\end{bmatrix}\cdot M_{z,des} \tag{4.5}$$

here β is the side-slip angle; l_f and l_r are the distance from the front/rear wheel to the center of mass, respectively; C_f and C_r are the tire cornering stiffness of the front/rear wheel, respectively; I_z is the rotational inertia on the z-axis; and $M_{z,des}$ is the desired yaw moment. One of the major drawbacks of the above equation is the side-slip angle, which is unobservable with sensors equipped in commercial vehicles. Thus, the equation of the motion of the bicycle model is rearranged as [26]:

$$\dot{\gamma}=-\frac{2C_fC_r}{C_f+C_r}\frac{(l_f+l_r)^2}{I_zV_x}\gamma+\frac{m(l_fC_f-l_rC_r)}{(C_f+C_r)I_z}a_y+\frac{2C_fC_r}{C_f+C_r}\frac{(l_f+l_r)}{I_z}\delta+\frac{1}{I_z}M_{z,des} \tag{4.6}$$

In accordance with sliding mode theory, the sliding surface and the sliding condition are described as [20]:

$$s_\gamma=\gamma-\gamma_{des},\qquad \frac{1}{2}\frac{d}{dt}{s_\gamma}^2=s_\gamma\dot{s}_\gamma\le-\eta_\gamma\left|s_\gamma\right| \tag{4.7}$$

where s_γ is the sliding surface; and η_γ is the sliding gain. From equation (4.7) and the vehicle states, the time derivative of the sliding surface is described as:

$$\begin{aligned}\dot{s}_\gamma &= \dot{\gamma} - \dot{\gamma}_{des} \\ &= -\frac{2C_fC_r}{C_f+C_r}\frac{(l_f+l_r)^2}{I_zV_x}\gamma + \frac{m(l_fC_f-l_rC_r)}{(C_f+C_r)I_z}a_y + \frac{2C_fC_r}{C_f+C_r}\frac{(l_f+l_r)}{I_z}\delta + \frac{1}{I_z}M_{z,des} - \dot{\gamma}_{des}\end{aligned}$$

(4.8)

To satisfy the sliding condition in equation (4.8), the desired yaw moment is described as:

$$M_{z,des} = I_z\dot{\gamma}_{des} - I_z\cdot\left\{-\frac{2\hat{C}_f\hat{C}_r}{\hat{C}_f+\hat{C}_r}\frac{(l_f+l_r)^2}{I_zV_x}\gamma + \frac{m(l_f\hat{C}_f-l_r\hat{C}_r)}{(\hat{C}_f+\hat{C}_r)I_z}a_y + \frac{2\hat{C}_f\hat{C}_r}{\hat{C}_f+\hat{C}_r}\frac{(l_f+l_r)}{I_z}\delta\right\} - \eta_\gamma\cdot sat(s_\gamma)$$

$$sat(s_\gamma) = \begin{cases} sgn(s_\gamma) & if\ |s_\gamma| > s_{th,\gamma} \\ s_\gamma & else \end{cases}$$

(4.9)

where $s_{th,\gamma}$ is the threshold to determine the $sat(s_\gamma)$ property; and $\hat{C}_i$ is the estimated tire cornering stiffness. However, tire cornering stiffness is varied and difficult to estimate. To minimize the error, the geometric mean of the tire cornering stiffness is considered [20]. Talvala et al. [19] proposed the dimensionless parameter η to indicate the saturation of the tire on the tire curve. The amounts of the parameter range from 0.3 to 0.5 at the fully saturated region. Thus, the estimated tire cornering stiffness is:

$$\hat{C}_i = \sqrt{1\cdot\eta_{sat}}\cdot\hat{C}_{i,o} \tag{4.10}$$

where η_{sat} is the dimensional parameter at the saturated region, which is set as 0.4 in this paper; and $\hat{C}_{i,o}$ is the tire cornering stiffness at the linear region. Because the normal load distribution between the front and rear axle is quite small, the effect of front/rear load transfer is not considered. The integrated chassis control algorithm can be improved with a tire cornering stiffness estimator.

4.2.2 Longitudinal Controller

The objective of the longitudinal controller is to reduce the longitudinal velocity error between the actual longitudinal velocity and the desired longitudinal velocity by the use of the desired longitudinal acceleration. The equation of motion in the longitudinal direction is described as:

$$a_x = \dot{v}_x + v_y\gamma = \frac{1}{m}\left(F_{x,des} - F_{yf}\delta\right) \tag{4.11}$$

where a_x is the longitudinal acceleration; v_y is the lateral velocity; m is the vehicle mass; $F_{x,des}$ is the desired longitudinal force; and F_{yf} is the lateral force of the front tire. Because an amount of the steering angle is almost within 0~10 degrees (0~ 0.17 rad), the effect of the lateral tire force could be considered as disturbance. Hence, because the lateral velocity of the vehicle is very small even at the limits, $v_y\gamma$ could also be considered as disturbance. Note that because the lateral force, steering angle and lateral velocity in typical maneuver have upper limit, both disturbance is norm-bounded uncertainties which can easily compensate with sliding mode theory. In accordance with sliding mode theory, the sliding surface and the sliding condition are described as [20]:

$$s_x = v_x - v_{x,des}, \qquad \frac{1}{2}\frac{d}{dt}s_x{}^2 = s_x\dot{s}_x \le -\eta_x\left|s_x\right| \tag{4.12}$$

where s_x is the sliding surface; and η_x is the sliding gain. From equation (4.12) and the vehicle state, the time derivative of the sliding surface is described as:

$$\dot{s}_x = \dot{v}_x - \dot{v}_{x,des} = \frac{1}{m}F_{x,des} - \dot{v}_{x,des} \tag{4.13}$$

To satisfy the sliding condition which is shown in equation (4.13), the desired longitudinal force can be calculated as:

$$\begin{aligned} F_{x,des} &= m\cdot\dot{v}_{x,des} - \eta_x\cdot sat(s_x) \\ sat(s_x) &= \begin{cases} sgn(s_x) & if\ \left|s_x\right| > s_{th,x} \\ s_x & else \end{cases} \end{aligned} \tag{4.14}$$

where $s_{th,x}$ is a threshold to determine the $sat(s_x)$ property.

4.3 Lower Level Controller: Optimal Coordination

The objective of the lower level controller is to optimally allocate the virtual control input to the 4WD and ESC actuators. From the upper level controller, the desired yaw moment and the desired longitudinal force are determined in the manner of sliding control theory. In the lower level controller, these desired forces and moments are optimally allocated while satisfying the target performance by minimizing designed cost function, as described in below.

Issue 1. Minimize the allocation error

- minimize the error between the virtual control input and the actuator control input

Issue 2. Combined slip monitoring based adaptation of the tire saturation penalty

- allocate the longitudinal force commands to a minimum at the wheel, which has a high tire saturation penalty

Issue 3. Follow the allocation guideline

- converge the optimal longitudinal force commands in the vicinity of the pre-defined, rule-based solution

Issue 4. Minimize unwilling braking

- minimize the use of braking torques of ESC

Issue 5. Actuator constraints

- consider the limit and rate limit of the actuators

The principal concept of optimal allocation is maximally utilizing the friction circle of each tire. The issues 2 and 3 are newly proposed in this paper. By following the allocation guideline and monitoring tire saturation with the tire saturation penalty, the vehicle could show enhanced maneuver performance at the limits.

4.3.1 Issue 1: Minimize the allocation error

The ideal relationship between the virtual control inputs and the actuator control input is described as:

$$\begin{cases} F_{x,des} = \underbrace{\left(F_{x,F,4WD} + F_{x,R,4WD}\right)}_{F_{x,4WD}} \\ \qquad\quad - \underbrace{\left(F_{x,FL,ESC} + F_{x,FR,ESC} + F_{x,RL,ESC} + F_{x,RR,ESC}\right)}_{F_{x,ESC}} \\ M_{z,des} = -\dfrac{t_w}{2} \cdot \left(F_{x,FL,ESC} - F_{x,FR,ESC} + F_{x,RL,ESC} - F_{x,RR,ESC}\right) \end{cases}$$

$$u(t) = \left[F_{x,F,4WD} \quad F_{x,R,4WD} \quad F_{x,FL,ESC} \quad F_{x,FR,ESC} \quad F_{x,RL,ESC} \quad F_{x,RR,ESC}\right]^T \tag{4.15}$$

where $F_{x,i,4WD}$ is the traction force command of the 4WD actuator; $F_{x,i,ESC}$ is the braking force command of the ESC actuator; t_w is the track width of the vehicle; and $u(t)$ is the actuator control input vector. In the matrix form, equation (4.15) is re-arranged as:

$$\underbrace{\begin{bmatrix} F_{x,des} \\ M_{z,des} \end{bmatrix}}_{v_1[2\times1]} = \underbrace{\begin{bmatrix} 1 & 1 & -1 & -1 & -1 & -1 \\ 0 & 0 & \frac{t_w}{2} & -\frac{t_w}{2} & \frac{t_w}{2} & \frac{-t_w}{2} \end{bmatrix}}_{B_1[2\times6]} \cdot \underset{u[6\times1]}{u(t)} \tag{4.16}$$

$$\text{minimize} \quad \left\|B_1 u(t) - v_1(t)\right\|$$

where v_1 is the virtual control input vector; and B_1 is the allocation matrix. In order to minimize the allocation error, the difference between the virtual control input and the summation of the actual control input in equation (4.16), $\left\|B_1 u(t) - v_1(t)\right\|$ is added to the cost function.

4.3.2 Issue 2: Combined slip monitoring based tire saturation penalty

To keep the tire in the stable region, the longitudinal force command might be allocated on the non-saturated tire. Numerous previous researches [4-7] minimize the tire workload to keep the tire stable, which is defined as:

$$(Tire\ workload\ at\ i\,th\ wheel) = \frac{\sqrt{{F_{x,i}}^2 + {F_{y,i}}^2}}{\mu F_{z,i}} \tag{4.17}$$

where $F_{\{x,y,z\},i}$ is the force of the i-th wheel in the longitudinal, lateral, and vertical direction, respectively; and μ is the tire-road friction coefficient. The monitor of the tire workload has shown improved performance at the limits. However, this method possesses two drawbacks. First, an estimation of the lateral tire force $F_{y,i}$ is a very challenging task in the experimental situation.

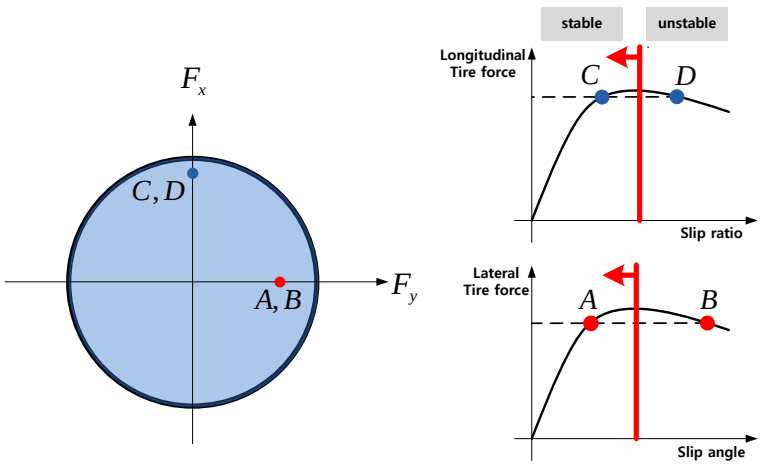

Figure 4.2. Drawback of the tire workload

Compared to tire forces, the combined slip is a kinematic variable and easier to estimate with vehicle parameters and state [27, 28]. Note that according to [27] and [28], in order to estimate side slip angle, vehicle dynamics should be considered. In this procedure in [27] and [28], lateral tire force of front/rear wheel should be estimated. However, to utilize tire workload for integrated chassis control at the limits, lateral tire force of four tires are needed. Moreover, to know lateral tire force of four tires, tire model parameters and estimated side slip angle are needed as seen in [29]. Thus, tire slip angles are needed to be estimated prior to tire lateral forces and relatively easy to be estimated. Second, the tire workload could not distinguish the saturation of the tire near the peak value. As seen in Fig. 2, points A and B indicate the same tire workload, but point A is stable and point B is unstable near the peak slip angle. Due to these drawbacks, tire force based tire saturation monitoring is not suitable for commercial vehicle. Thus, to compensate for these drawbacks, a combined slip based tire saturation penalty is newly tried in this paper.

Although the tire saturation penalty is similar to the tire workload, it is a combined slip based tire saturation index. The combined slip is defined as [30]:

$$\sigma_i = \sqrt{{\sigma_{x,i}}^2 + {\sigma_{y,i}}^2}$$
$$\sigma_{x,i} = \frac{\kappa_i}{1+\kappa_i},\ \sigma_{y,i} = \frac{\tan\alpha_i}{1+\kappa_i} \tag{4.18}$$

where σ_i is the combined slip of i-th wheel; $\sigma_{\{x,y\},i}$ is the modified, i-th tire slip ratio and slip angle, respectively; κ_i is the slip ratio of i-th wheel; and α_i is the slip angle of i-th wheel. In this paper, which is focused on the control algorithm, it is assumed that the reasonable combined slip information is provided by the combined slip estimator. This combined slip should be compared with the peak combined slip value as normalized tire force in the tire workload to evaluate the risk of tire saturation. The peak combined slip value is difficult to set as a constant value because it varies with the tire-road friction coefficient, the vertical force, and the tire state [30]. Thus, a reasonable tire peak slip should be obtained to evaluate the tire saturation index of each tire. The brush tire model is simple, yet it is widely used in the vehicle control field, from lateral force estimation [31] to drifting [32]. In the brush tire model, the peak tire slip is defined as [30]:

$$\sigma_{peak,i} = \frac{3\mu F_{z,i}}{C_{i,o}} \tag{4.19}$$

where $\sigma_{peak,i}$ is the peak tire slip; and $C_{i,o}$ is the tire cornering stiffness at the linear region.

The tire saturation penalty is defined in the manner of hyperbolic penalty [33], which is function of a tire combined slip, a tire peak slip, and a friction limit of each tire as:

$$k_i = \left[\left(-a_{hyper}\cdot\frac{(|\hat{\sigma}_i| - 0.5\cdot\hat{\sigma}_{peak,i})}{\hat{\sigma}_{peak,i}} + \sqrt{\left\{a_{hyper}\cdot\frac{(|\hat{\sigma}_i| - 0.5\cdot\hat{\sigma}_{peak,i})}{\hat{\sigma}_{peak,i}}\right\}^2 + {b_{hyper}}^2}\right)\right] \Big/ \bar{\mu}\hat{F}_z \tag{4.20}$$

where k_i is the tire saturation penalty of i-th wheel; $\bar{\mu}$ is the tire-road friction coefficient; and a_{hyper} and b_{hyper} are tuning parameters, which adjust the slope and y-value of $0.5\cdot\hat{\sigma}_{peak,i}$, respectively, of the hyperbolic penalty function. The graph of the hyperbolic penalty is presented in Fig. 3. The penalty function has two asymptote, $y = 2a_{hyper}|\hat{\sigma}_i|$ and $y = 0$. As increasing a_{hyper} and b_{hyper}, the slope

of hyperbolic penalty and y-value of $0.5 \cdot \hat{\sigma}_{peak,i}$ become increasing. In this paper, a_{hyper} and b_{hyper} are tuned as 10 and 2, respectively, by trial and error. The penalty function could be defined with a log barrier function or secant trigonometrical function. These functions, however, abruptly vary after a threshold value, and this abrupt change could result in a sudden change in torque command, which is not desirable and could make the vehicle unstable. Thus, in this paper, the hyperbolic penalty function is adopted as the tire saturation penalty function.

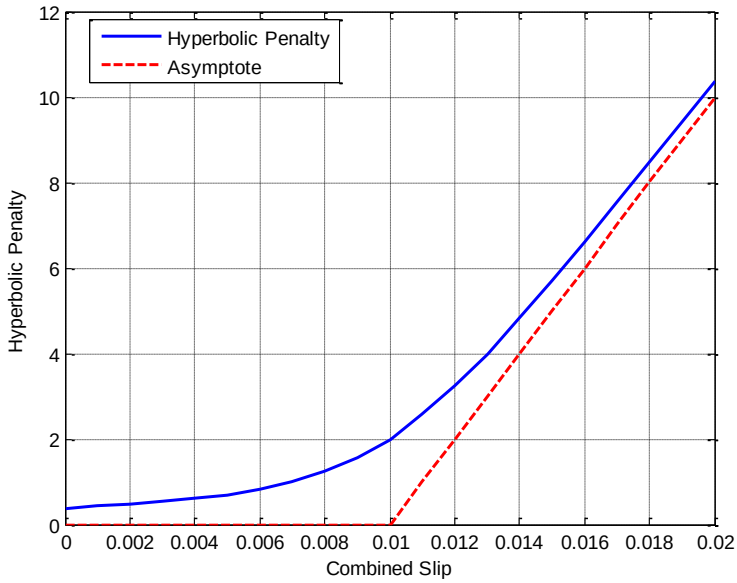

Figure 4.3. Hyperbolic penalty : $F_z = 5000N,\ \mu = 1,\ \sigma_{peak} = 0.02$

To optimally allocate longitudinal force command to a minimum at the wheel, which has a high tire saturation penalty, cost should be increased when the amount of the tire saturation function is increased. Thus, the resultant penalty is summarized as:

$$\begin{bmatrix} k_{FL} & 0 & 0 & 0 \\ 0 & k_{FR} & 0 & 0 \\ 0 & 0 & k_{RL} & 0 \\ 0 & 0 & 0 & k_{RR} \end{bmatrix} \cdot \underbrace{\overbrace{\begin{bmatrix} 0.5 & 0 & -1 & 0 & 0 & 0 \\ 0.5 & 0 & 0 & -1 & 0 & 0 \\ 0 & 0.5 & 0 & 0 & -1 & 0 \\ 0 & 0.5 & 0 & 0 & 0 & -1 \end{bmatrix}}^{B_{Longi}}}_{\begin{bmatrix} F_{x.FL} & F_{x.FR} & F_{x.RL} & F_{x.RR} \end{bmatrix}^T} \cdot u(t) = \underset{[4\times6]}{B_{TSP}} \cdot \underset{[6\times1]}{u(t)}$$

$$\text{minimize} \quad \left\| B_{TSP} u(t) \right\| \tag{4.21}$$

where B_{Longi} is the longitudinal force matrix; and B_{TSP} is the tire saturation penalty matrix. In order to minimize the longitudinal force command allocation on the saturated tire, the magnitude of the above equation should be minimized. Thus, the tire saturation penalty term, $\|B_{TSP}u(t)\|$, is added to the cost function. However, if only the tire saturation penalty is used to allocate the longitudinal tire force, the optimal solution is highly gain/case-sensitive and does not produce a reasonable, consistent solution at the limits. In previous researches [8, 9], the gain is tuned as varied velocity or lateral acceleration. However, this gain-scheduled system also cannot guarantee consistent performance in various situation cases. Thus, in this paper, the allocation guideline, which is the sub-optimal solution of the time minimization problem [3], leads the optimal solution to the vicinity of the sub-optimal solution.

4.3.3 Issue 2: Issue 3: Follow the allocation guideline

The objective of the allocation guideline is to lead the optimal longitudinal force command in the vicinity of the pre-defined, rule-based solution. The pre-defined, rule-based solution is the sub-optimal solution of the time minimization problem [3]. In previous research, Castro et al. [3] proposed the time optimal solution, which can be obtained from off-line optimal control. Hence, to apply the solution on-line, they proposed a simple, sub-optimal torque distribution ratio as:

$$\gamma_0 = \left(1 + \frac{a_x}{a_x\cos(\delta) + a_y\sin(\delta)} \frac{\hat{F}_{z,RL} + \hat{F}_{z,RR}}{\hat{F}_{z,FL} + \hat{F}_{z,FR}}\right)^{-1},$$

$$\gamma_1 = \frac{\hat{F}_{z,FR}}{\hat{F}_{z,FL} + \hat{F}_{z,FR}}, \quad \gamma_2 = \frac{\hat{F}_{z,RR}}{\hat{F}_{z,RL} + \hat{F}_{z,RR}}$$

(4.22)

where γ_0 is the front/rear distribution ratio; and γ_1 and γ_2 are the front-axle and rear-axle distribution ratio, respectively. The distribution ratios, given by the sub-optimal solution, are approximately the ratio of each wheel's vertical force to vehicle weight. In other words, the given ratios are nearly the ratio of friction circle radius to friction limit of the vehicle. This result is quite straightforward in point of vehicle handling at the limits, which maximally utilizes the friction circle. Previous research [3] has shown that the sub-optimal solution is similar to the off-line optimal solution. The remarkable point is that the distribution ratio consists of a measurable signal (a_x, a_y, δ) and vertical forces of each tire, which are easy to

reasonably estimate .

To follow the allocation guideline, the allocation guideline term is arranged as:

$$v_{AG}(t)=\begin{bmatrix}F_{FL,AG,des}\\F_{FR,AG,des}\\F_{RL,AG,des}\\F_{RR,AG,des}\end{bmatrix}=\begin{bmatrix}\gamma_o\cdot(1-\gamma_1)\cdot F_{x,des}\\\gamma_o\cdot\gamma_1\cdot F_{x,des}\\(1-\gamma_o)\cdot(1-\gamma_2)\cdot F_{x,des}\\(1-\gamma_o)\cdot\gamma_2\cdot F_{x,des}\end{bmatrix}=\underbrace{\overbrace{\begin{bmatrix}0.5&0&-1&0&0&0\\0.5&0&0&-1&0&0\\0&0.5&0&0&-1&0\\0&0.5&0&0&0&-1\end{bmatrix}}^{B_{Longi}}\cdot u(t)}_{\begin{bmatrix}F_{x.FL}&F_{x.FR}&F_{x.RL}&F_{x.RR}\end{bmatrix}^T}$$

$$\text{minimize}\quad \left\|B_{Longi}u(t)-v_{AG}(t)\right\| \tag{4.23}$$

where $F_{i,AG,des}$ is the desired allocation guideline of i-th wheel.

In addition, by adding the allocation guideline, the optimal solution becomes robust and consistent against weighting gain and simulation case. Although the sub-optimal solution exhibits consistency at the limits, uncertainties and disturbances can make the vehicle unstable in real situations. This problem could be compensated by considering the tire saturation penalty, which is described above. This interaction between the allocation guideline and tire saturation penalty enables limit handling of the vehicle.

4.3.4 Issue 4: Minimize unwilling braking

Unwilling braking should be minimized at the limits, because unwilling braking results in unwilling deceleration and tire wear. To minimize unwilling braking, the braking input term is described as:

$$\underbrace{\overbrace{\begin{bmatrix}0&0&-1&0&0&0\\0&0&0&-1&0&0\\0&0&0&0&-1&0\\0&0&0&0&0&-1\end{bmatrix}}^{W_{u1}}\cdot u(t)}_{\begin{bmatrix}F_{x.FL,ESC}&F_{x.FR,ESC}&F_{x.RL,ESC}&F_{x.RR,ESC}\end{bmatrix}^T}=W_{u1}\cdot u(t) \tag{4.24}$$

$$\text{minimize}\quad \left\|W_{u1}\cdot u(t)\right\|$$

4.3.5 Issue 5: Actuator constraints

Actuator constraints should be considered in the control algorithm for a physically feasible solution, especially an integrated chassis control algorithm for

limit handling which uses a friction circle of each wheel maximally. The actuator limits of each wheel due to the tire-road friction limit can be described as:

$$\hat{F}_{x,\max,i} = \sqrt{\left(\hat{\mu} \cdot \hat{F}_{z,i}\right)^2 - \hat{F}_y} \tag{4.25}$$

where $\hat{F}_{x,\max,i}$ is the estimated longitudinal friction circle limit. However, the lateral force in the actuator constraints is difficult to estimate in real situations. Thus, by removing the lateral tire force, the actuator constraints are considered as:

$$\hat{F}_{x,\max,i} = \sqrt{\left(\bar{\mu} \cdot \hat{F}_{z,i}\right)^2}$$

$$\begin{cases} U_{\min} = \begin{bmatrix} 0 & 0 & 0 & 0 & 0 & 0 \end{bmatrix}^T \\ U_{\max} = \begin{bmatrix} \hat{F}_{x,\max,FL} + \hat{F}_{x,\max,FR} \\ \hat{F}_{x,\max,RL} + \hat{F}_{x,\max,RR} \\ \hat{F}_{x,\max,FL} \\ \hat{F}_{x,\max,FR} \\ \hat{F}_{x,\max,RL} \\ \hat{F}_{x,\max,RR} \end{bmatrix} \end{cases} \tag{4.26}$$

where $U_{\min}$ and $U_{\max}$ is the lower and upper bound of the actuator constraint, respectively. This over-estimated actuator limit due to neglecting the lateral tire force may cause commanding a larger longitudinal force, i.e., physically infeasible longitudinal force, than the physical maximum value. However, due to the tire saturation penalty issue of the optimal coordination, the proposed algorithm commands a physically feasible longitudinal force, unlike other control algorithms. The actuator constraints are not only upper- and lower-bound, but also rate-limited. The rate-limit is the upper- and lower-bound of the time derivative of the control input as:

$$r_{\min} \le \dot{u}(t) \le r_{\max} \tag{4.27}$$

where $r_{\min}$ is the lower rate limit; and $r_{\max}$ is the upper rate limit. If the time derivative of the control input is approximated as:

$$\dot{u}(t) \approx \frac{u(t) - u(t - T_{sampling})}{T_{sampling}} \tag{4.28}$$

where $T_{sampling}$ is the sampling time of the algorithm, then the actuator rate limit can be considered by modifying actuator constraint as [34

$$\begin{cases} U_{\min} = \max\left[U_{\min}, u(t - T_{sampling}) + T_{sampling} \cdot r_{\min} \right] \\ U_{\max} = \min\left[U_{\max}, u(t - T_{sampling}) + T_{sampling} \cdot r_{\max} \right] \end{cases} \tag{4.29}$$

From equations (4.26) and (4.29), the over-estimated upper- /lower-bound of the actuator limits and rate limit of the actuators are considered in the optimal coordination.

4.3.6 Optimal coordination

Consequently, from issue 1 to issue 5, the cost function can be arranged in weighted least square (WLS) form as:

$$\begin{aligned} u(t) &= \arg\min_{U_{\min} \le u \le U_{\max}} \begin{bmatrix} \zeta_{u1} \cdot \left\| W_{u1} \cdot u \right\|^2 + \zeta_{v1} \cdot \left\| W_{v1} \cdot \left(B_1 \cdot u - v_1 \right) \right\|^2 \dots \\ + \zeta_{v2} \cdot \left\| W_{v2} \cdot \left(B_{TSP} \cdot u \right) \right\|^2 + \zeta_{v3} \cdot \left\| W_{v3} \cdot \left(B_{Longi} \cdot u - v_{AG} \right) \right\|^2 \end{bmatrix} \\ &= \arg\min_{U_{\min} \le u \le U_{\max}} \left\{ \left\| \underbrace{\begin{pmatrix} \zeta_{v1}^{\frac{1}{2}} \cdot W_{v1} \cdot B_1 \\ \zeta_{v2}^{\frac{1}{2}} \cdot W_{v2} \cdot B_{TSP} \\ \zeta_{v3}^{\frac{1}{2}} \cdot W_{v3} \cdot B_{Longi} \\ \zeta_{u1}^{\frac{1}{2}} \cdot W_{u1} \end{pmatrix}}_{A} \cdot u - \underbrace{\begin{pmatrix} \zeta_1^{\frac{1}{2}} \cdot W_{v1} \cdot v_1 \\ 0 \\ \zeta_3^{\frac{1}{2}} \cdot W_{v3} \cdot v_{AG} \\ 0 \end{pmatrix}}_{b} \right\|^2 \right\} \\ &= \arg\min_{U_{\min} \le u \le U_{\max}} \left\{ \left\| A \cdot u - b \right\|^2 \right\} \end{aligned} \tag{4.30}$$

where $W_{\{u,v\},i}$ is the diagonal weighting matrix to differently weight on control inputs; and $\zeta_{\{u,v\},i}$ is the weighting factor to differently weight on issues which are proposed in Section 2.3. The above WLS form optimization problem is solved with the active set algorithm [35 The overall scheme of the optimal coordination is shown in Fig. 4. From the virtual input, i.e., desired longitudinal force and yaw

moment, the optimal longitudinal force distribution is determined by minimizing the cost function. The control algorithm calculates optimal 4WD/ESC control inputs $\begin{bmatrix} F_{x,F,4WD} & F_{x,R,4WD} & F_{x,FL,ESC} & F_{x,FR,ESC} & F_{x,RL,ESC} & F_{x,RR,ESC} \end{bmatrix}^T$. Each calculated actuator control input is exerted to 1st order based 4WD/ESC actuator model. Note that the 1st order delays for 4WD/ESC are selected as 0.03 sec and 0.06 sec respectively to mimic actual actuator. 4WD/ESC actuators exert $\begin{bmatrix} F_{x,F,4WD} & F_{x,R,4WD} \end{bmatrix}$ and $\begin{bmatrix} F_{x,FL,ESC} & F_{x,FR,ESC} & F_{x,RL,ESC} & F_{x,RR,ESC} \end{bmatrix}$ respectively. Consequently, wheel longitudinal force for each wheel is determined as $\sum_{j=\{L,R\}} \sum_{i=\{F,R\}} \left(\frac{1}{2} \cdot F_{x,i,4WD} - F_{x,ij,ESC} \right)$.

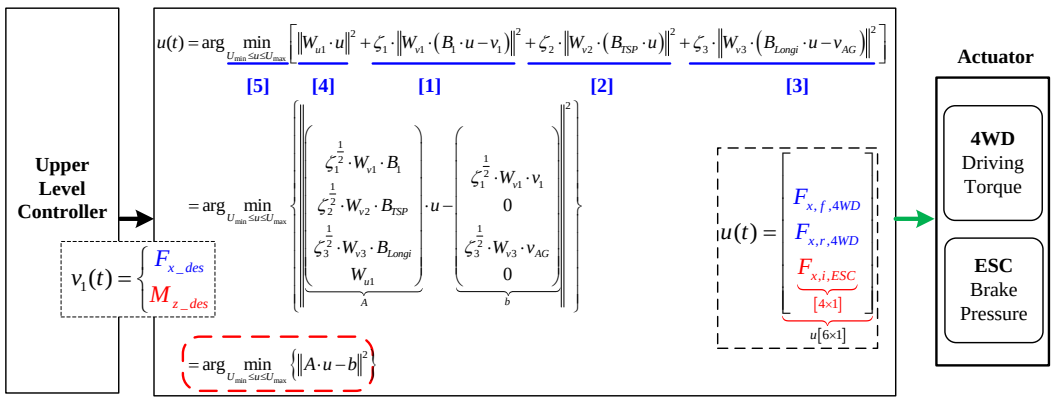

Figure 4.4. Overall scheme of optimal coordination

4.4. Simulation Results

All of the simulations in this paper are performed with Matlab/Simulink and Carsim. In Section 4.4.1, the individual allocation issue of the lower level controller, especially allocation guideline and tire saturation penalty, is investigated by comparing the proposed integrated control algorithm (ICA) with imperfect ICAs. Circular turning with constant acceleration is conducted in Section 4.4.1 to investigate the desired road tracking performance with stable motion. In Section 4.4.2, the proposed integrated chassis control algorithm is compared with the Base and ESC-equipped vehicle. The ESC-equipped vehicle evenly distributes the yaw moment by using differential braking. Double lane change (DLC) with constant acceleration is conducted in Section 4.4.2 to investigate the performance of the algorithm in the situation in which combined slip exists. In Section 4.4.3, a comprehensive simulation on racing track is performed. The proposed algorithm is validated and compared with uncontrolled/ESC-equipped vehicle. Vehicle parameters of Carsim F class have been modified to obtain similar dynamic characteristics of the target vehicle, i.e., a 2000 kg weighted luxury sedan.

4.4.1. Comparison with other ICAs

In this section, comparison of the proposed ICA with other ICAs is conducted on circular turning (radius = 85 m, counterclockwise turning) with constant acceleration in order to investigate the vehicle in the combined slip situation. The simulation is conducted with a 50 kph initial speed, 0.4 g acceleration, and 0.5 sec preview driver model. The simulation result is shown in Figs. 4.5-4.10. ICAs are discriminated as original ICA, ICA with allocation guideline, and ICA with allocation guideline and tire saturation penalty, depending on which issues are considered. The original ICA only considers issues 1, 4, and 5 in Section 2.3. The ICA with allocation guideline considers issues 1, 2, 4, and 5. Finally, the ICA with allocation guideline and tire saturation penalty is the proposed algorithm which considers all five issues.

As seen in trajectories of the vehicle in Fig. 4.5 and lateral error in Fig. 4.6, Base vehicle and the vehicle with original ICA cannot track the desired road. Lateral error becomes larger as the velocity increases, and even the steering angle in Fig. 4.6 becomes larger. In contrast, as seen in the trajectories of vehicles in Fig. 4.5 and lateral error in Fig. 4.6, the ICA with allocation guideline and the proposed ICA tracks the desired road well (lateral error < 1m). Thus, at least, to track the desired road at the limits, the allocation guideline should be added. However, as seen in the steering command in Fig. 4.6, in the case of the ICA with allocation

guideline, to keep the vehicle on the desired road, the steering command given by driver model oscillates. Due to the oscillating steering angle command, velocity and errors are in oscillation, which is difficult situation to deal with for a driver.

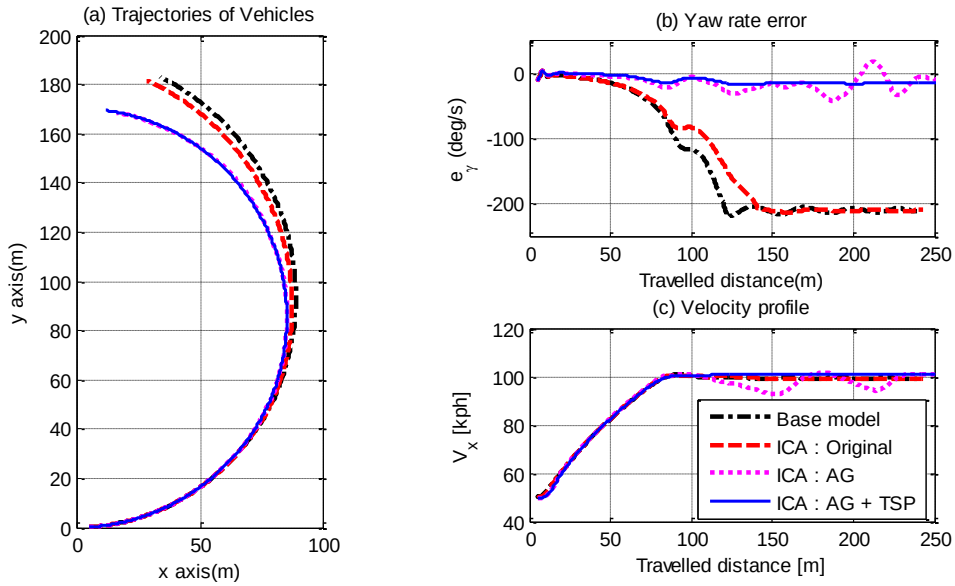

Figure 4.5. Comparison of the proposed ICA with imperfect ICAs

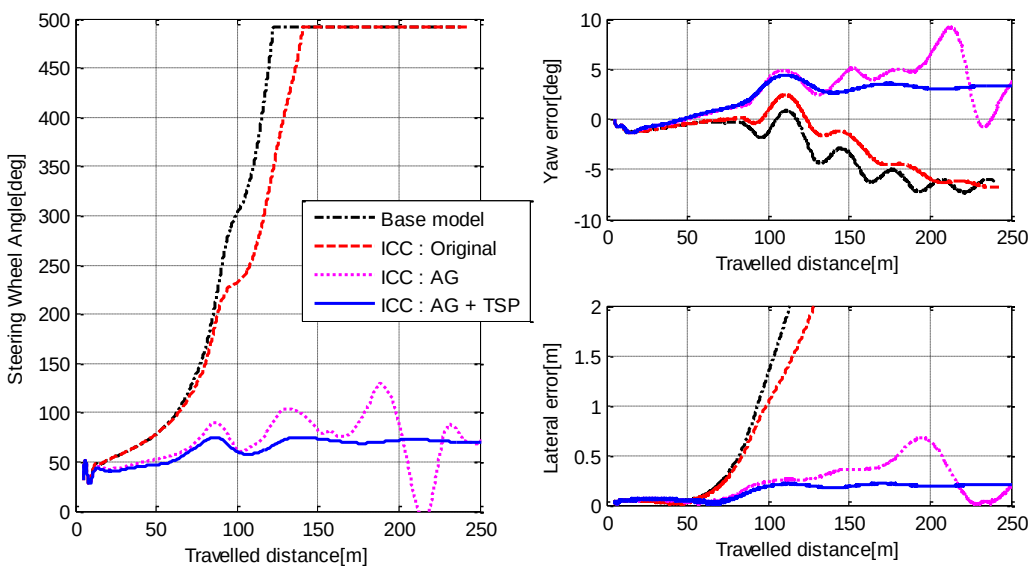

Figure 4.6. Desired road tracking performance

In order to determine the reason for the steering command oscillation, force and slip circle diagrams are presented, as seen in Figs. 4.7 and 4.8, respectively. Both the force and slip diagram are normalized with their maximum values, the friction limit and peak slip of the brush tire model, respectively. As seen in Fig. 4.7, the

force cannot physically exceed its maximum value. Moreover, both of the ICA with allocation guideline and the proposed ICA algorithms maximally utilize the friction circle. However, as seen in Fig. 4.8, the normalized combined slip of the ICA with allocation guideline largely exceeds its limit; whereas, the combined slip of the proposed ICA remains near the limit. This excessive combined slip leads the vehicle to enter an unstable region. Because the tire combined slip of the ICA with allocation guideline is much larger than that of the proposed ICA, the tire saturation penalty of the ICA with allocation guideline is also larger. This constitutes evidence to prove the concept of the tire saturation penalty, as shown in Fig. 4.2. The tire forces are similar, yet the combined slip is in an unstable region. From the tire workload point of view, because the tire forces of the ICAs are similar, the vehicle is not in a problematic situation; however, from the tire saturation penalty point of view, because the combined slip of the ICA with allocation guideline exceeds the peak slip, the vehicle experiences a serious problem. Thus, with the tire saturation penalty, an integrated chassis control algorithm can realize whether or not the tire is in an unstable region and then keep the tire stable at the limits.

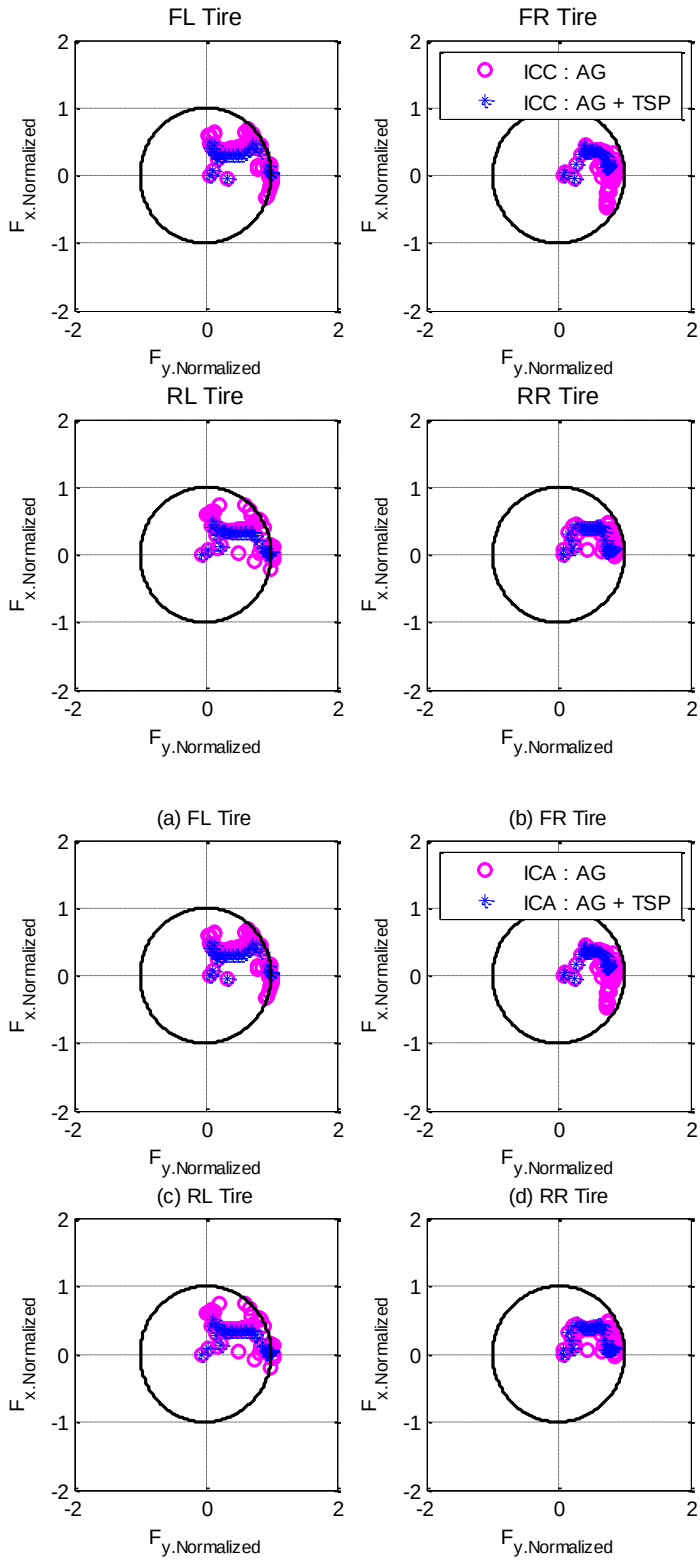

Figure 4.7. Force diagram comparison

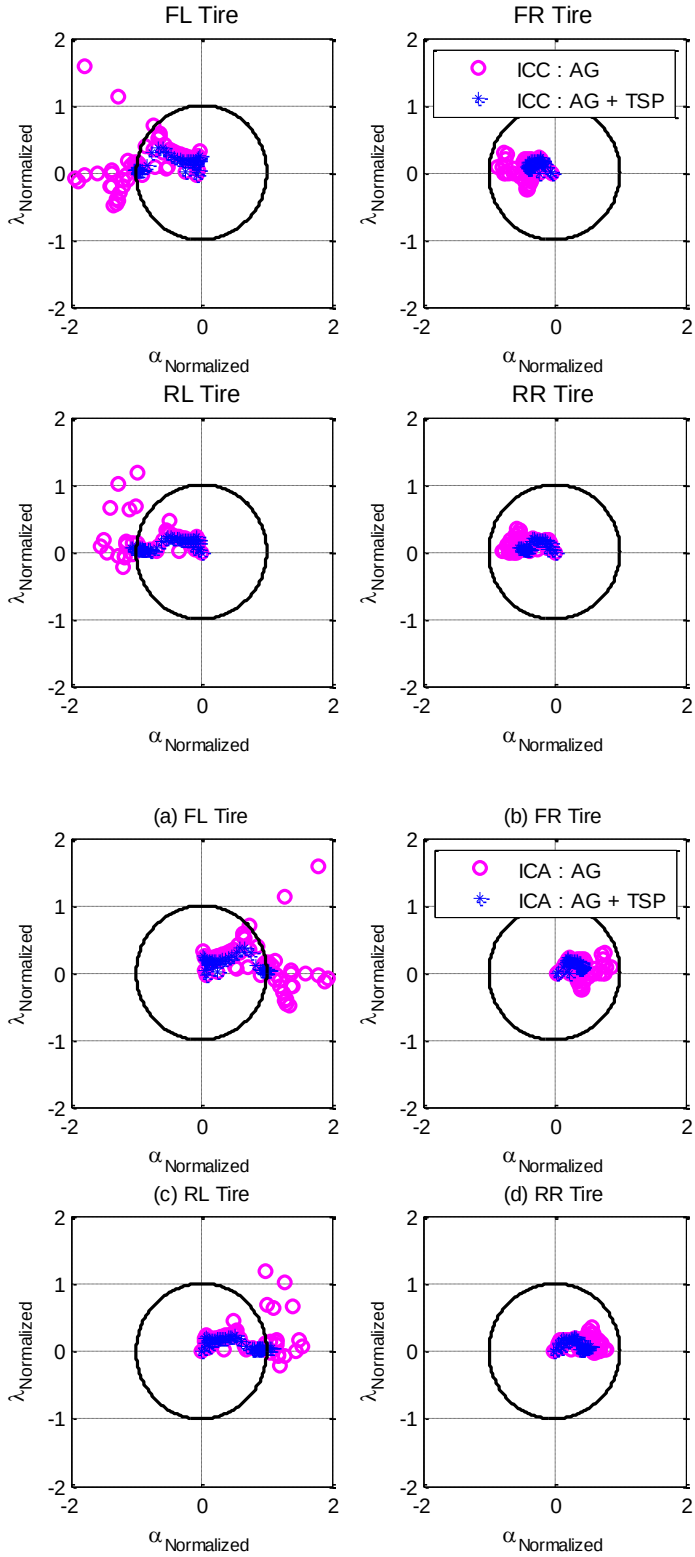

Figure 4.8. Slip circle comparison

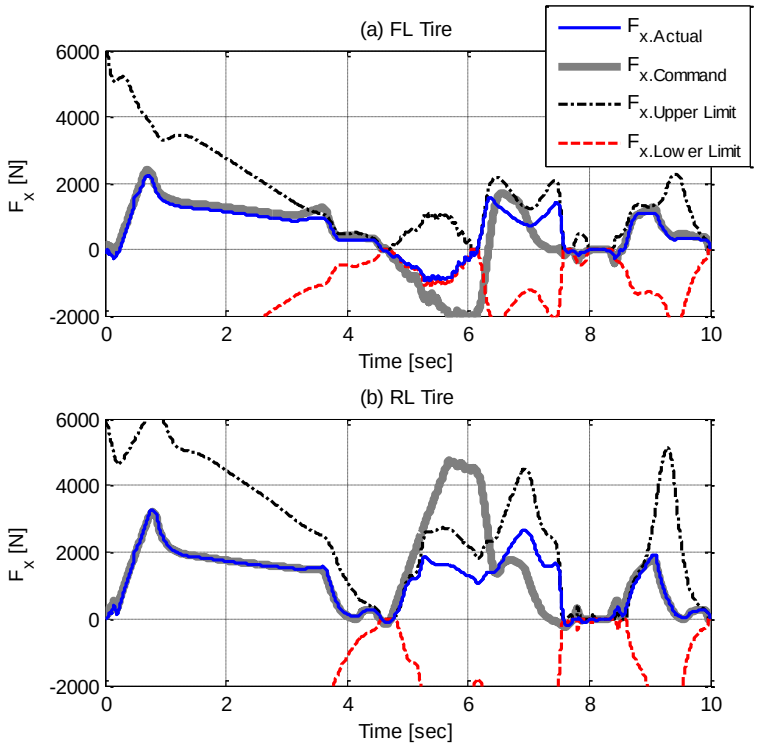

Figure 4.9. ICA with allocation guideline: Time history of forces

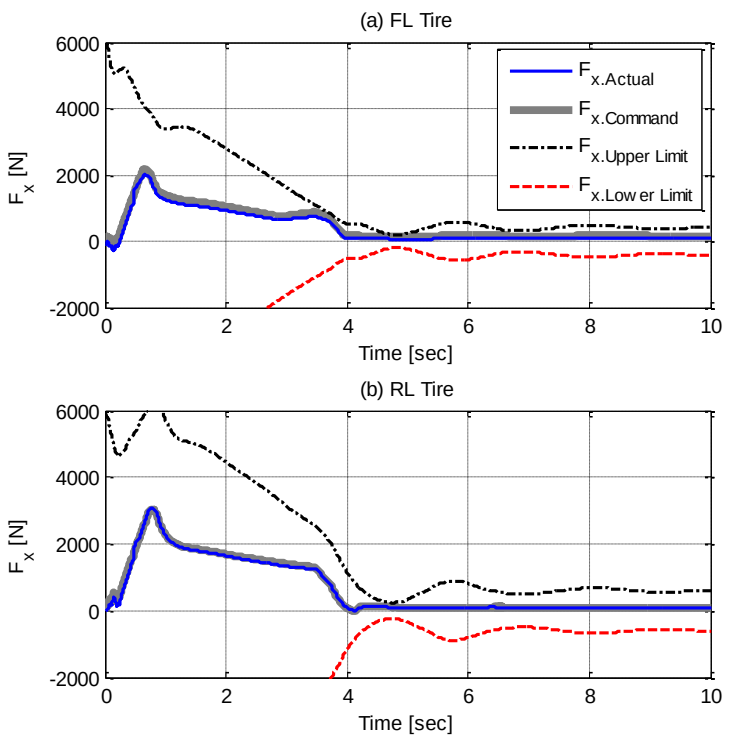

Figure 4.10. Proposed ICA (AG + TSP): Time history of forces

The time histories of the left tire forces of the ICA with allocation guideline and the proposed ICA are presented in Figs. 4.9 and 4.10, respectively. There are three signals: Fx,actual, Fx,command, and Fx,limit. Fx,actual is the actual longitudinal force of each tire, Fx,command is the commands of ICA, and Fx,limit is the physical friction limit of longitudinal force as equation (4.25), $\hat{F}_{x,\max,i} = \sqrt{\left(\hat{\mu}\cdot\hat{F}_{z,i}\right)^2 - \hat{F}_y}$. In the case of the ICA with allocation guideline, the ICA commands a physically infeasible longitudinal force, which is larger than Fx,limit, and the longitudinal force signals fluctuate, as seen in Fig. 4.9. This excessive Fx,command, due to the over-estimated actuator constraint described in Section 4.3.5, results in excessive combined slip, as seen in Fig. 4.8. Consequently, this excessive combined slip leads the vehicle to an unstable region and oscillation in the yaw direction. In contrast to ICA with allocation guideline, the proposed ICA commands a physically feasible longitudinal force, as seen in Fig. 4.10. The Fx,command and Fx,actual are maintained in the Fx,limit. Moreover, as shown in Fig. 4.8, the combined slip of the each wheel is maintained near the peak slip.

4.4.2. Comparison with unequipped vehicle

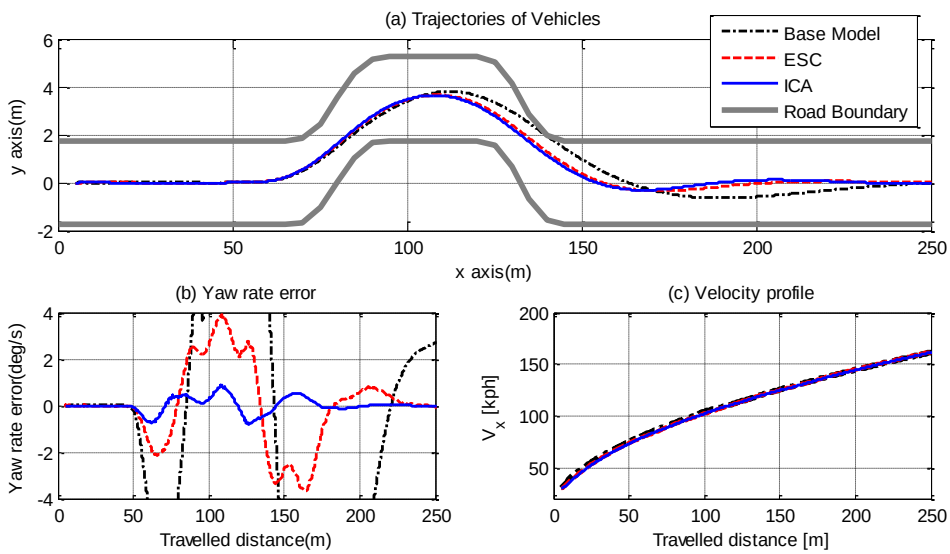

Figure 4.11. Comparison the proposed ICA with base model and ESC

In this section, a comparison of the proposed integrated control algorithm (ICA) with base and ESC-equipped vehicles is conducted on double-lane change with constant acceleration in order to investigate the vehicle in the combined slip

situation. The simulation is conducted with a 30 kph initial speed, 0.4 g acceleration, and 0.5 sec preview driver model. The simulation result is shown in Fig. 4.11.

As seen in velocity profile of Fig. 4.11, the vehicle tracks the desired velocity well. However, as seen in the trajectories of the vehicles, the unequipped vehicle and the ESC-equipped vehicle disturb the driver's intention, i.e., the desired yaw rate. The remarkable point is the proposed algorithm well recovers vehicle lateral stability after aggressive maneuver as seen in yaw rate error after travelled distance 160m. After travelled distance 160m, the vehicle finishes lane changes and returns to the original lane. The base model and ESC-equipped vehicle is fail or difficult to recover from lateral instability as seen in overshoot or undershoot on yaw rate error. In contrast to these vehicles, the vehicle with ICA quickly recovers from lateral instability.

This simulation result could show that the proposed algorithm exhibits better performance than base model and ESC-equipped vehicles. However, the above results cannot show the maximum performance of the algorithms. To validate the overall performance of the algorithm, circular turning (radius=85m) with constant acceleration is repeatedly conducted. The simulation cases are divided into acceleration and deceleration cases. In the acceleration case, simulation is conducted with a 50kph initial speed and pre-set longitudinal acceleration. In the deceleration case, simulation is conducted with a 120kph initial speed and pre-set longitudinal deceleration. The maximum performance of each case is measured when the vehicle deviates from the desired road or fails to track the desired velocity in terms of lateral acceleration. The simulation results are shown in Fig. 12. Each single point in Fig. 12 is the maximum lateral acceleration with the specific longitudinal acceleration of the vehicles via simulation studies. The blue dashed-line is the vehicle limit, and the black long- and short-dashed lines are the theoretical limits of the base model.

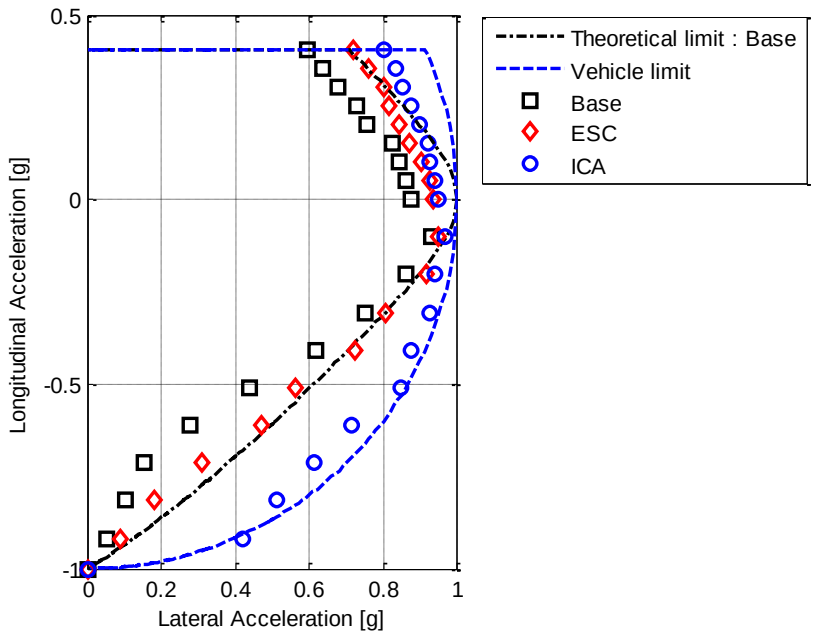

Figure 4.12. Maximum performance: Base model, ESC, and the proposed ICA

As illustrated in Fig. 4.12, the ESC algorithm exhibits improved performance than the base model. This improvement of the ESC is due to the differential braking. However, since tire saturation is not considered in the ESC, the maximum performance of the ESC is smaller than vehicle limit. By considering tire saturation as the proposed ICA algorithm the maximum performance of the vehicle can be improved as illustrated in Fig. 4.12. Consequently, the proposed algorithm can utilize the larger lateral acceleration with the same longitudinal acceleration. This larger maximum performance enables greater longitudinal speed at cornering and eventually minimizes lap time on racing track.

4.4.3. Comprehensive Simulation on Racing Track

In this section, a comparison of the proposed integrated control algorithm (ICA) with Base model and ESC-equipped vehicles is conducted on corners 3-6 of Korea International Circuit [36]. To validate ICA performance on racing track, the driver model on previous section. The desired path and the velocity profiles are pre-determined prior to the simulations. The desired path is determined by the path-fitting algorithm [37] with respect to a skillful driver's driving trajectory. Subsequently, the optimal velocity profile can be obtained from the fitted curvature profile [38]. In the process, the capability of accelerations has to be known. In this paper, the velocity profiles are calculated from the three different capability

envelopes, which are analyzed in Section 4.4.2. Note that the maximum speed is set as 200kph. The simulation results are shown in Fig. 4.13 and 4.14.

The overall simulation results are shown in Fig. 4.13. To analyse simulation results in detail, vehicle acceleration states and path tracking errors on corner 3/corner 4-6 are respectively shown in Fig. 4.14. Trajectories and path tracking errors of three algorithms are similar as seen in Fig. 4.13 (a) and Fig. 4.14 respectively. Moreover, because the speed at each corner cannot exceed friction limit (μg), the cornering speed at each corner apex is identical as seen in black circle of Fig. 4.13 (b). However, due to the difference in maximum performance of three algorithms as seen in Fig. 4.12, the velocity profile of algorithms are different as seen in Fig. 4.13 (b). Most prominently, the velocity of ICA algorithm is faster than other algorithm when vehicle starts to decelerate. In contrast to Base and ESC algorithms, the proposed ICA algorithm well utilizes the friction limit of each wheel and is able to provide larger deceleration during negotiating corner, i.e., combined acceleration case. Thus, as seen in Fig 4.14 (a) and (e), the ICA can decelerate late and maintain the large deceleration even in combined acceleration case, whereas Base and ESC should decelerate early to reduce their speed to cornering speed at corner apex. Consequently, ICA reduces lap time by 5.5% (3.89sec) compared with the base model.

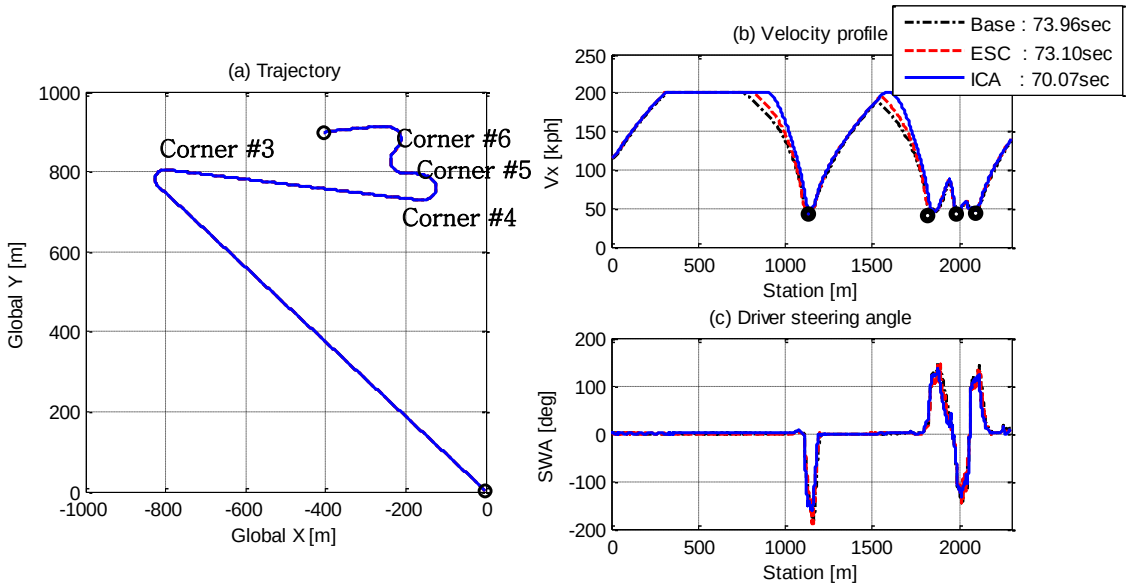

Figure 4.13. Overall simulation results on racing track

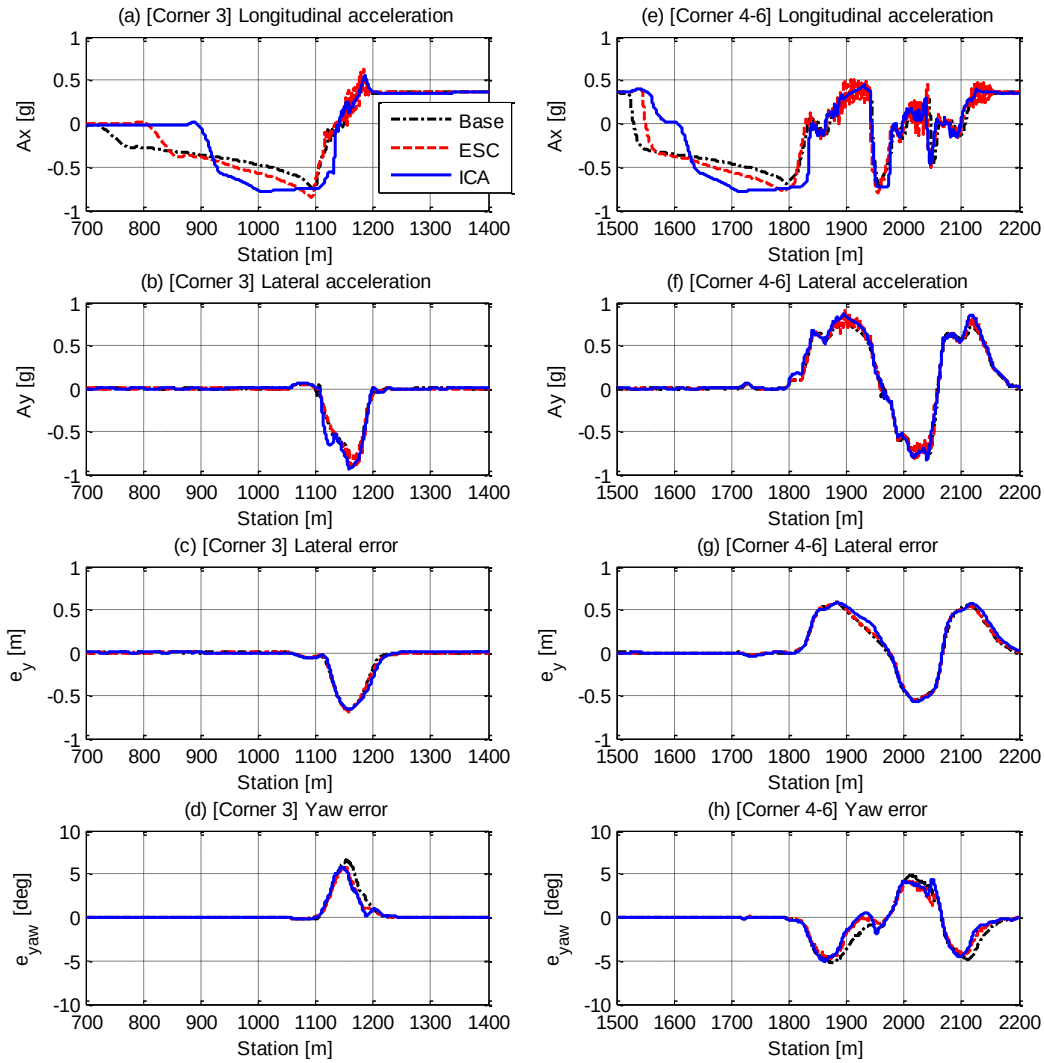

Figure 4.14. Comparison ICA with Base and ESC equipped vehicle on racing track

Chapter 5

Development of Integrated Chassis Control Algorithm of ESC, 4WD, ECS and ARS for Enhanced Limit Handling

For enhanced limit handling of the vehicle, vertical force of each tire is important and necessary to manage because vertical force of each tire directly represents friction limit of each tire. Thus, by integrating vertical force control chassis modules with ESC/4WD integrated chassis control algorithm, limit handling performance of the vehicle can be enhanced.

The architecture of the integrated chassis control consists of three main layers as seen in Fig. 5.1. First, from driver command, the supervisor determines desired longitudinal velocity, yaw rate, and roll angle. Second, from desired value and vehicle states, the upper level controller determines the desired longitudinal force, yaw moment, and roll moment in the sliding control manner to guarantee robust stability against model uncertainty. Third, from desired force/moment, the lower level controller optimally allocates the actual control input for 4WD/ESC and ECS/ARS. Note that to avoid nonlinearity of cost function, 4WD/ESC control algorithm and ECS/ARS are separately designed. Because 4WD/ESC integrated chassis control algorithm is already described in Chapter 4, ECS/ARS algorithm is only presented in this Chapter 5.

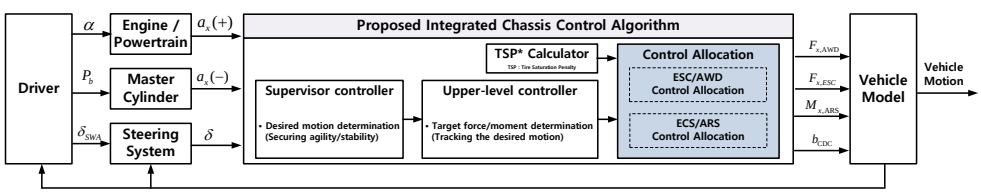

Figure 5.1. Block diagram of the control algorithm

5.1. Supervisor

For ECS/ARS integrated algorithm, supervisor determine desired roll angle based on vehicle states. The desired roll angle is designed with relationship between lateral acceleration and roll angle in the steady state condition[39].

$$\phi = k_{Roll} a_y$$

where ϕ is the roll angle; and k_{Roll} is the tuning parameter, called as roll sensitivity.

Note that principal purpose of ARS is to minimize roll angle of the vehicle, the tuning parameter k_{Roll} of the vehicle is set to present small roll angle than base vehicle.

5.2. Upper Level Controller

The role of the upper level controller is to calculate the generalized force(Longitudinal force/ Yaw moment/ Roll moment) to track the desired motion. To design robust controller against model uncertainty, disturbance and noise, the generalized force are determined in the sliding mode control theory manner.

The objective of the desired yaw moment is to stabilize roll angle error dynamics. The desired roll moment is designed with the equation of motion of the roll based roll model in the sliding control manner.

$$I_x\ddot{\phi} = -K_\phi\phi + M_\phi + m_s h_s a_y \tag{5.1}$$

where I_x is the roll inertia; K_ϕ is the whole roll stiffness; ϕ is the roll angle; M_ϕ is the roll moment; m_s is the mass of sprung mass; and h_s is the roll height. With sliding mode theory, the sliding surface and the sliding condition are described as [20]:

$$s_\phi = \left(\dot{\phi} - \dot{\phi}_{des}\right) + \lambda_\phi\left(\phi - \phi_{des}\right), \qquad \frac{1}{2}\frac{d}{dt}s_\phi^{\,2} = s_\phi\dot{s}_\phi \le -\eta_\phi\left|s_\phi\right| \tag{5.2}$$

where s_ϕ is the sliding surface; and η_ϕ is the sliding gain. Similarly, to satisfy sliding condition, desired roll moment is calculated as:

$$M_{\phi,des} = I_x\left(\ddot{\phi}_{des} + \lambda_\phi\dot{\phi}_{des}\right) - m_s h_s a_y - I_x\left(\lambda_\phi + K_\phi\right)\dot{\phi} + \left(K_\phi - I_x K_\phi\lambda_\phi\right)\phi - k_\phi sat(s_\phi) \tag{5.3}$$

$$sat(s_\phi) = \begin{cases} sign(s_\phi) & if\ \left|s_\phi\right| > s_{th,\phi} \\ \left|s_\phi\right| & else \end{cases}$$

5.3. ECS/ARS Control Allocation

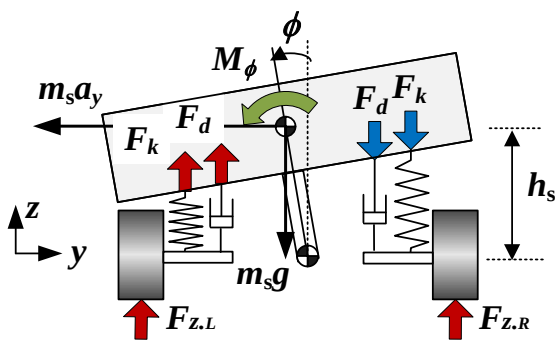

Figure 5.2. Roll center based roll dynamic model

To avoid nonlinearity of optimization problem, the control allocation of the vertical force control module is separately designed. Because the actuator control inputs of ECS and ARS are normalized damping coefficient and front/rear roll moment, the relationship between these actuator inputs and vertical force should be formulated before formulating cost function of ECS/ARS control allocation,

5.3.1. Relationship between actuator inputs and vertical force

As seen in Fig 5.2 and from the equations of the motion, the vertical force of each tire at the steady state can be represented as below:

$$\begin{aligned} F_{z.iL} &= \underbrace{k_s x_{iL} + c_{iL}\dot{x}_{iL}}_{\text{Suspension}} - \underbrace{\left(\frac{1}{t_w}M_{i\phi} + \frac{1}{t_w}K_i\phi\right)}_{\text{Roll effect}} + \underbrace{\frac{mg}{4}}_{\text{Static load}} \\ F_{z.iR} &= \underbrace{k_s x_{iR} + c_{iR}\dot{x}_{iR}}_{\text{Suspension}} + \underbrace{\left(\frac{1}{t_w}M_{i\phi} + \frac{1}{t_w}K_i\phi\right)}_{\text{Roll effect}} + \underbrace{\frac{mg}{4}}_{\text{Static load}} \quad (i = F, R) \end{aligned} \tag{5.4}$$

where k_s is the suspension spring stiffness; $c_{i(L/R)}$ is the damping coefficient, which is control input of ECS; K_i is the roll stiffness; $x_{i(F/R)}$ is the suspension compression distance; and $M_{i\phi}$ is the roll moment, which is control input of ARS. Consequently, the vertical force of the each tire can be written in matrix form.

$$\begin{aligned} & u = \begin{pmatrix} M_{\phi.f} & M_{\phi.r} & c_{FL} & c_{FR} & c_{RL} & c_{RR} \end{pmatrix}^T \\ \Rightarrow & \underbrace{\begin{pmatrix} F_{z,fl} \\ F_{z,fr} \\ F_{z,rl} \\ F_{z,rr} \end{pmatrix}}_{F_z} = \underbrace{\begin{pmatrix} -1/t_w & 0 & \dot{x}_{fl} & 0 & 0 & 0 \\ 1/t_w & 0 & 0 & \dot{x}_{fr} & 0 & 0 \\ 0 & -1/t_w & 0 & 0 & \dot{x}_{rl} & 0 \\ 0 & 1/t_w & 0 & 0 & 0 & \dot{x}_{rr} \end{pmatrix}}_{B_z} u - \underbrace{\begin{pmatrix} -k_s x_{fl} + K_f\phi/t_w - mg/4 \\ -k_s x_{fr} - K_f\phi/t_w - mg/4 \\ -k_s x_{rl} + K_r\phi/t_w - mg/4 \\ -k_s x_{rr} - K_r\phi/t_w - mg/4 \end{pmatrix}}_{v_{dynamics}} \end{aligned} \tag{5.5}$$

where B_z and $v_{dynamics}$ are matrix and vector name respectively. With relationship between vertical force and actuator inputs, design of ECS/ARS control allocation module is intuitive.

There are 4 issue in ECS/ARS control allocation.

Issue 1. Minimize the allocation error : reduce the error between the generalized force and the sum of actuator control input

Issue 2. Minimize variance of tire saturation penalty : allocate the vertical force to minimize variance of the tire saturation penalty

Issue 3. Minimize yaw rate error by controlling front/rear lateral load transfer distribution: allocate the optimal vertical force command to reduce yaw rate error based on nonlinearity of tire

Issue 4. Actuator constraint

5.3.2. Issue 1 : Minimize the allocation error

To track desired roll moment, which is calculated in upper level controller to track desired roll angle, the first row of the below equation should be satisfied.

$$
\begin{aligned}
&u = \begin{pmatrix} M_{\phi.f} & M_{\phi.r} & c_{FL} & c_{FR} & c_{RL} & c_{RR} \end{pmatrix}^T \\
&\underbrace{\begin{pmatrix} M_{\phi,des} \\ 0 \end{pmatrix}}_{v_{Direct}} = \underbrace{\begin{pmatrix} 1 & 1 & -t_w\dot{x}_{fl}/2 & t_w\dot{x}_{fr}/2 & -t_w\dot{x}_{rl}/2 & t_w\dot{x}_{rr}/2 \\ 0 & 0 & \dot{x}_{fl} & \dot{x}_{fr} & \dot{x}_{rl} & \dot{x}_{rr} \end{pmatrix}}_{W_{Direct}} u
\end{aligned}
\tag{5.6}
$$

The left hand side of the first row is desired roll moment and the right hand side is generated roll moment by ECS/ARS. The second row is designed to maintain sum of damping force from ECS zero. This row is added to prevent z direction of sprung mass oscillation. In order to minimize the allocation error, $\left\| W_{Direct}u(t) - v_{Direct}(t) \right\|$ is added to the cost function.

5.3.3. Issue 2 : Minimize variance of tire saturation penalty

To keep the tire stable, the vertical force of the saturated tire should become larger as seen in definition of tire workload (4.17) and tire saturation penalty (4.20). However, the sum of vertical force is almost constant. Thus, if controller increases vertical force of highly saturated tire to reduce tire saturation, other tires become unstable due to constant sum of vertical force. Then, controller decides to increase vertical force of other tires. Consequently, if cost function is designed to minimize sum of tire saturation penalty as 4WD/ESC, this cost function can cause oscillation. Thus, the controller should concentrate on minimization of variance of tire saturation penalty, not the sum of the penalty.

To minimize variance of tire saturation penalty, the cost function is designed in matrix form as:

$$
\underbrace{\begin{pmatrix} -\sigma_{fl} & -\sigma_{fr} & -\sigma_{rl} & -\sigma_{rr} \end{pmatrix}}_{W_{TSP}} \begin{pmatrix} F_{z,fl} \\ F_{z,fr} \\ F_{z,rl} \\ F_{z,rr} \end{pmatrix} = W_{TSP}\left(B_z u - v_{dynamics} \right)
\tag{5.7}
$$

where $\sigma_{ij} = \left[k(\alpha_{ij}, \lambda_{ij}) - E\left(k(\alpha_{ij}, \lambda_{ij}) \right) \right]$

where W_{TSP} is the matrix, defined in the equation (5.7); B_z and $v_{dynamics}$ are defined in equation (5.5); and $k(\alpha_{ij}, \lambda_{ij})$ is the tire saturation penalty, which is defined in the equation (4.20). As seen in equation (5.5), as σ_{ij}, which indicates variance of the tire saturation, become larger in ij-th tire, the vertical force of ij-th tire become larger to minimize the norm of the equation (5.5). In order to minimize the allocation error, $\left\| W_{TSP}\left(B_z u - v_{dynamics} \right) \right\|$ is added to the cost function.

5.3.4. Issue 3: Minimize yaw rate error by controlling front/rear lateral load transfer distribution

Due to the convexity of tire curve, by distributing lateral load transfer, which is difference between left and right tire, vertical force control module can minimize yaw rate error. Large lateral load transfer decreases axle lateral tire force. In previous research [40], to control yaw rate, 2nd order polynomial tire model is adopted. This methodology, however, is difficult to apply in real situation because the parameters of the tire model are unknown. To overcome this problem, in other previous researches [9, 41], yaw rate error based qualitative way have been used. In this paper, the controller is also designed with using yaw rate error based status index.

Yaw rate error based status index is defined as:

$$I_{status} = (\gamma_{des} - \gamma) \cdot sign(\gamma)$$
$$\begin{cases} I_{status} > 0 & understeer \\ I_{status} < 0 & oversteer \end{cases} \tag{5.8}$$

From status index, the front/rear roll moment distribution ratio is determined as:

$$\varepsilon = 0.5 - K_p I_{status} - K_I \int I_{status} dt \tag{5.9}$$

$$\Delta F_z \rightarrow \Delta F_{z,f} = \varepsilon \cdot \Delta F_z$$
$$\Delta F_{z,r} = (1-\varepsilon) \cdot \Delta F_z$$

Due to convexity of lateral load transfer and vertical force tire curve, increment of lateral load transfer causes decrement of axle lateral tire force. If steering characteristics of the vehicle is understeer, distribution ratio becomes less than 0.5 and lateral load transfer of front axle decreases. Thus, front axle lateral force increase, while rear axle lateral force decrease. Consequently, this unbalance of front and rear lateral tire force generates yaw moment to reduce understeer tendency.

To minimize the yaw rate error with this scheme, the matrix form cost function is suggested as:

$$\underbrace{\begin{pmatrix} 1-\varepsilon & 1-\varepsilon & 0 & 0 \\ 0 & 0 & -\varepsilon & -\varepsilon \end{pmatrix}}_{W_{load}} \cdot \begin{pmatrix} F_{z.FL} \\ F_{z.FR} \\ F_{z.RL} \\ F_{z.RR} \end{pmatrix} = W_{load} \left(B_z u - v_{dynamics} \right) \tag{5.10}$$
$$= (1-\varepsilon) \cdot \Delta F_{z,f} - \varepsilon \cdot \Delta F_{z,r}$$

To minimize the equation (5.10), the front/rear lateral load transfer should satisfy the relationship in the equation (5.9). In order to minimize the allocation error, $\left\| W_{load} \left(B_z u - v_{dynamics} \right) \right\|$ is added to the cost function.

5.3.5. Issue 4: Actuator constraint

Similar to 4WD/ESC control allocation, to allocate physically feasible commands, the actuator upper/lower bound and rate limit bound is considered. The only difference of the ECS/ARS with 4WD/ESC is that the upper/lower bound depend on actuator limit.

5.3.6. Optimal Coordination

From issue 1 to issue 5, the cost function can be arranged in weighted least square (WLS) form as:

$$
\begin{aligned}
u(t) &= \arg\min_{U_{\min}\le u\le U_{\max}} \begin{bmatrix} +\zeta_{v1}\cdot\left\|W_{Direct}\cdot\left(B_z u - v_{dynamics}\right)\right\|^2 \cdots \\ +\zeta_{v2}\cdot\left\|W_{TSP}\cdot\left(B_z u - v_{dynamics}\right)\right\|^2 + \zeta_{v3}\cdot\left\|W_{load}\cdot\left(B_z u - v_{dynamics}\right)\right\|^2 \end{bmatrix} \\
&= \arg\min_{U_{\min}\le u\le U_{\max}} \left\{ \left\| \underbrace{\begin{pmatrix} \zeta_{v1}^{\frac{1}{2}}\cdot W_{Direct}\cdot B_z \\ \zeta_{v2}^{\frac{1}{2}}\cdot W_{TSP}\cdot B_z \\ \zeta_{v3}^{\frac{1}{2}}\cdot W_{load}\cdot B_z \end{pmatrix}}_{A}\cdot u - \underbrace{\begin{pmatrix} \zeta_{v1}^{\frac{1}{2}}\cdot W_{Direct} \\ \zeta_{v2}^{\frac{1}{2}}\cdot W_{TSP} \\ \zeta_{v3}^{\frac{1}{2}}\cdot W_{load} \end{pmatrix} v_{dynamics}}_{b} \right\|^2 \right\} \\
&= \arg\min_{U_{\min}\le u\le U_{\max}} \left\{ \left\| A\cdot u - b \right\|^2 \right\}
\end{aligned}
\tag{5.11}
$$

where $\zeta_{v,i}$ is the weighting factor to differently weight on issues. The above WLS form optimization problem is solved with the active set algorithm [35].

5.4. Comparison and validation

The proposed algorithm in this paper is validated via Matlab /Simulink and Carsim co-simulation in PC level. The vehicle model is mid-size sedan(sprung mass : 1700kg, l_f=1.4m, l_r=1.6m), which handling characteristics set to neutral steer at the linear region. There are two kinds of simulation scenario. Both scenarios are conducted on mu=1 road. First scenario is constant/varying speed double lane change(DLC). In DLC scenario, the proposed ICC(4WD/ESC/ECS/ARS) algorithm is compared to base model and 4WD/ESC equipped vehicle to evaluate effectiveness of integration of individual chassis module. Second scenario is accelerating circular turning case. In this scenario, the proposed ICC is compared to 4WD/ESC/ARS integrated controller, which is proposed in [41], to evaluate the performance of the proposed cost function and integration framework. For fair comparison, ECS is not controlled in this simulation. However, the integration framework of longitudinal/vertical force control module and novel cost function are the main contribution of this paper. Thus, evaluation and comparison the proposed ICC without ECS with ICC in [41] is meaningful.

5.4.1. Open-loop Double Lane Change

In this scenario, the comparison the proposed ICC algorithm (4WD/ESC/ECS/ARS) with base vehicle and 4WD/ESC equipped vehicle is conducted. Note that the 4WD/ESC algorithm is nothing but the proposed algorithm without ECS/ARS system. The purpose of this scenario is to evaluate effectiveness of integration of individual chassis module. There are two kinds of constant speed 75kph and accelerating from 40kph to 75kph with 0.3g.

The simulation result for constant speed DLC is shown in Fig. 5.3 and Fig. 5.4. As seen in Fig 5.3. (b), same open-loop steering command is applied to three different systems, and, as seen in Fig 5.3. (d), this scenario is nearly limit situation (max : ~0.9g). The responses of the systems, however, are different. As seen in Fig 5.3, the proposed ICC well manipulate given chassis module to track the desired motion. First of all, because the proposed ICC system has degree of freedom in roll motion, peak-to-peak roll angle is significantly minimized as seen in Fig 5.3. (e), compared to other systems. Second, the yaw rate error of the proposed ICC is stabilized more than the other systems as seen in Fig 5.3. (g). From root-mean-squrae(RMS) error analysis, compared to base model('No control'), the chassis control module can reduce nonlinearity in handling characteristics. It is shown that 4WD/ESC module can reduce yaw rate error. However, 4WD/ESC Integrated control system causes yaw rate error oscillation, which can be easily shown in limit handling situation due to small tire damping.[27,28] In contrast to 4WD/ESC integrated control system, the proposed algorithm reduces yaw rate error oscillation as seen in red dash line of Fig 5. (g). Moreover, as seen in legend of Fig 5. (g), RMS error of the proposed algorithm is less than that error of 4WD/ESC integrated system.

The reason of performance enhancement can be analyzed in tire saturation penalty. The maximum stable tire saturation penalty can be defined by simply replacing combined slip in the equation (25) with the equation (24). Then, tire saturation penalty is normalized with the maximum stable tire saturation penalty

and defined normalized tire saturation penalty as tire saturation index as seen in y axis of the Fig. 5.4. Because the tire saturation penalty is not zero with zero combined slip, the tire saturation index is not zero. As seen in Fig. 6, in the case of base vehicle, the tire saturation index of specific tire is significantly larger than 1 and oscillating. With 4WD/ESC integrated control system, the sum of the tire saturation penalty is minimized. Thus, tire saturation index is more stable, yet some tires have near maximum tire saturation penalty which implies that the unstable tire. In contrast to base model('No control') and 4WD/ESC, the proposed ICC algorithm effectively keep the tire saturation index below the maximum by minimizing sum and variance of the tire saturation penalty.

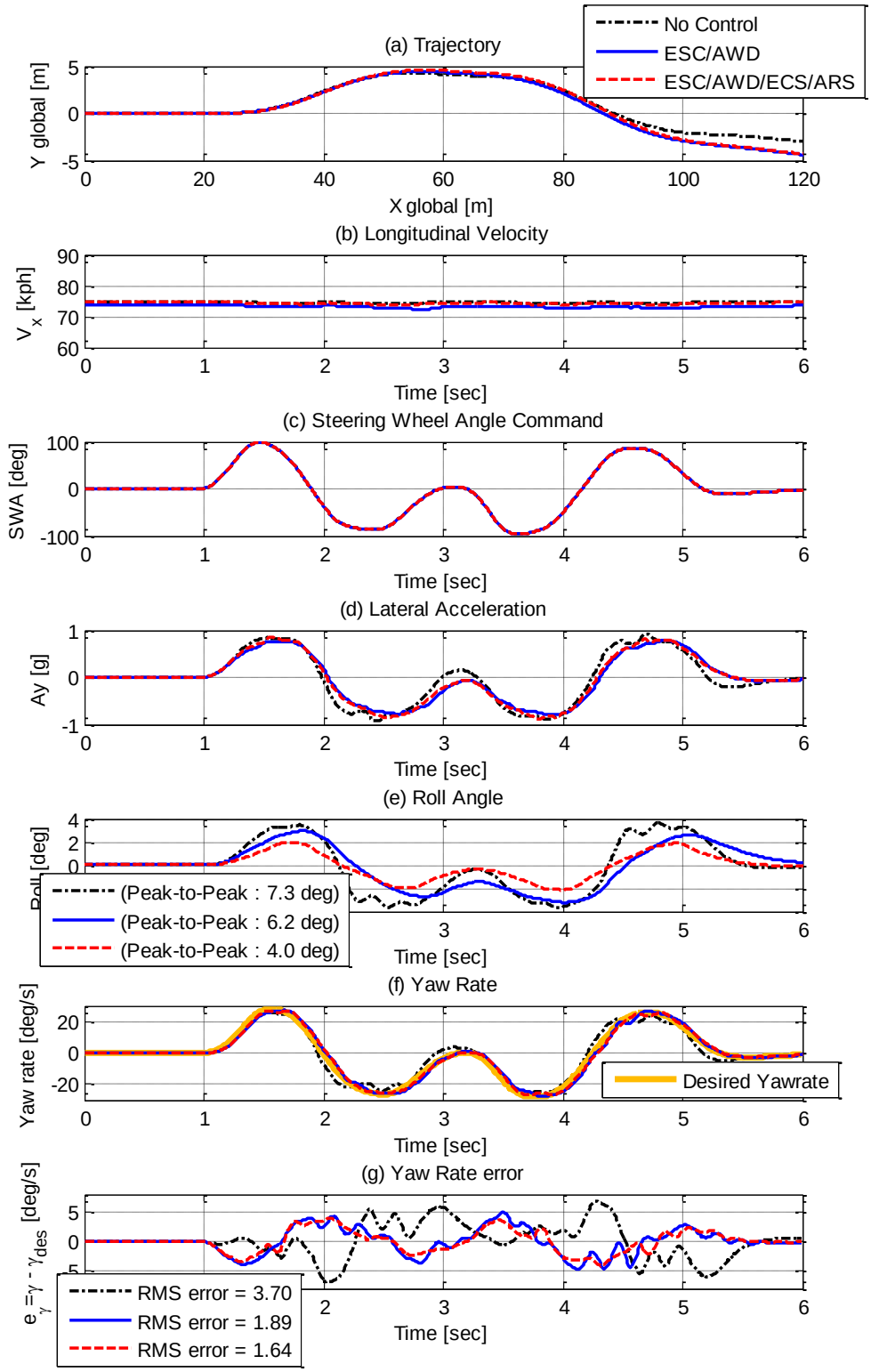

Figure 5.3. Overall vehicle performance at constant speed DLC

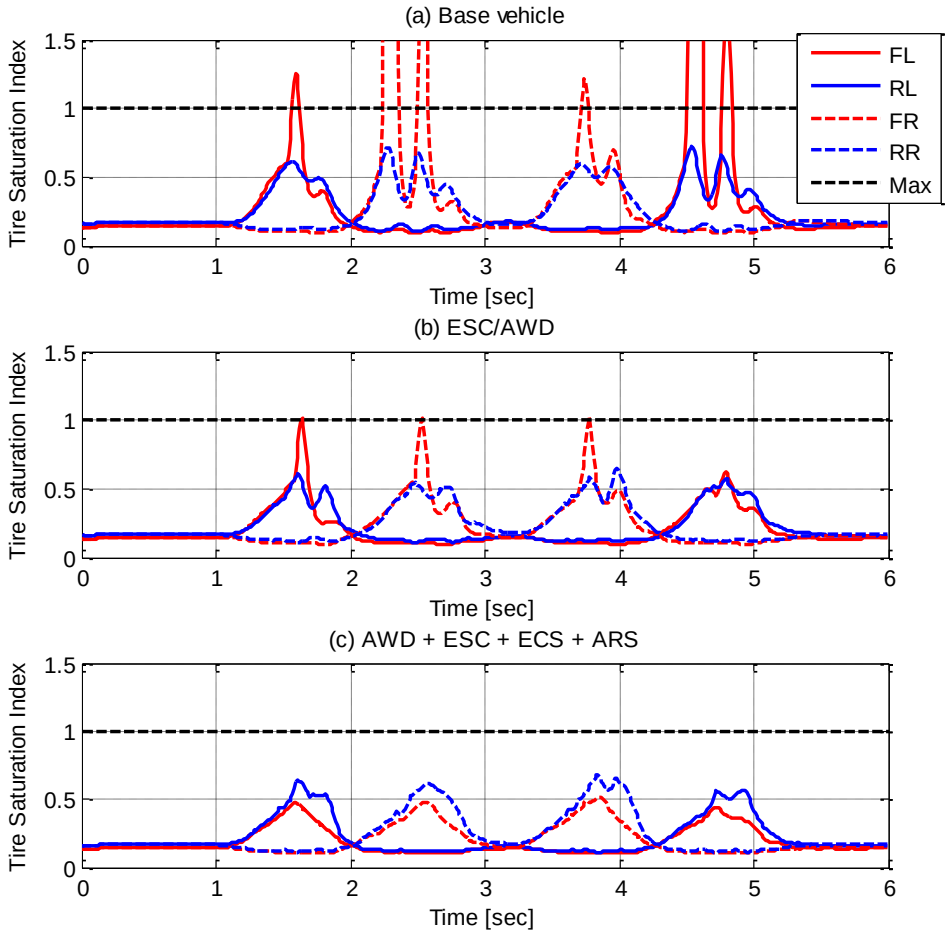

Figure 5.4. Tire saturation index at constant speed

To evaluate the proposed algorithm with combined acceleration case, the DLC scenario with same open-loop steering condition and constant longitudinal acceleration is conducted. The simulation results are shown in Fig. 5.5 and Fig. 5.6. As seen in 4~5sec in Fig 5.5. (g), the yaw rate error oscillation is reduced by the proposed ICC algorithm. Moreover, the RMS error is reduced. Similarly, as seen in Fig. 5.6, the proposed ICC algorithm maintains tire saturation stable.

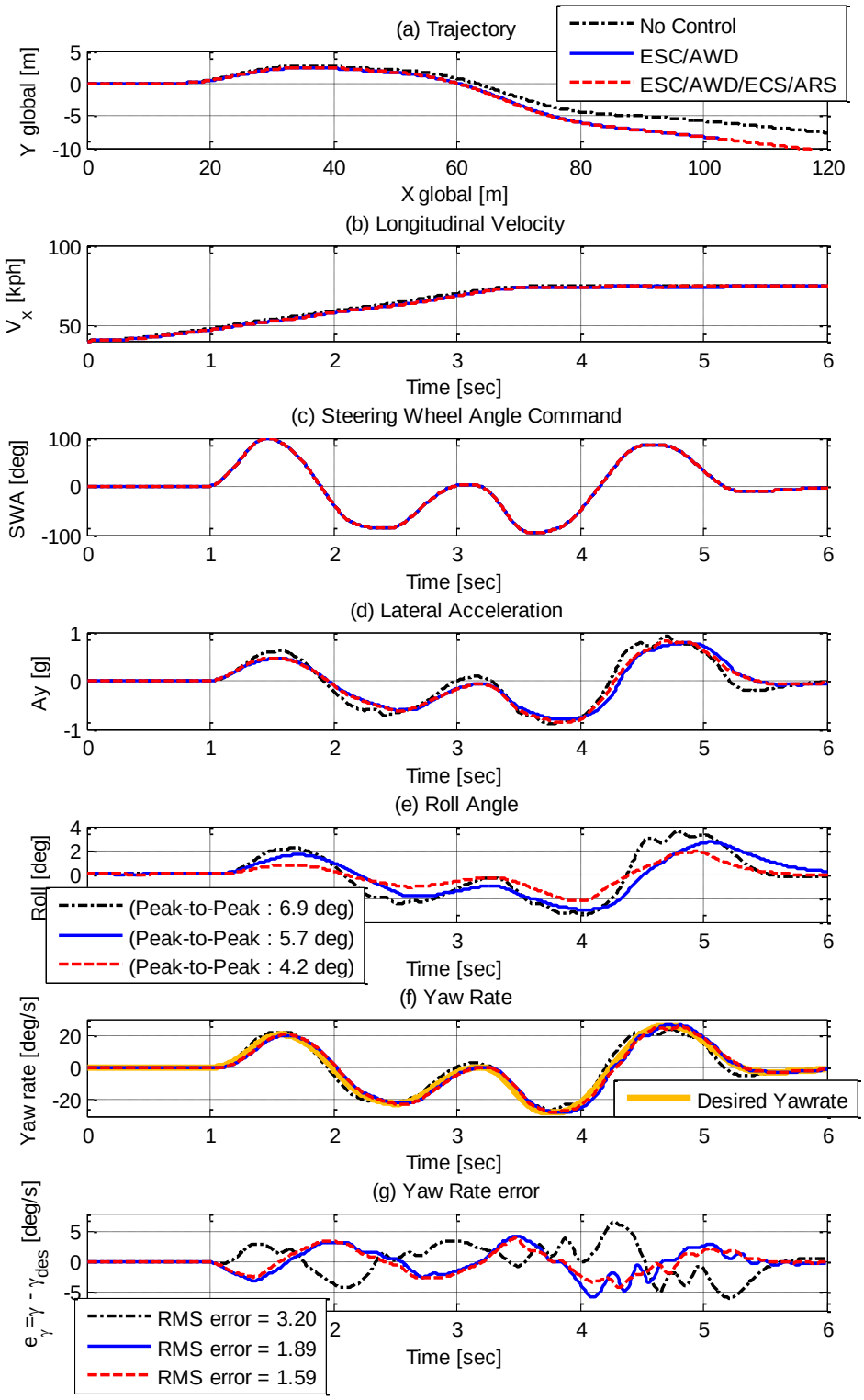

Figure 5.5. Overall vehicle performance at accelerating DLC

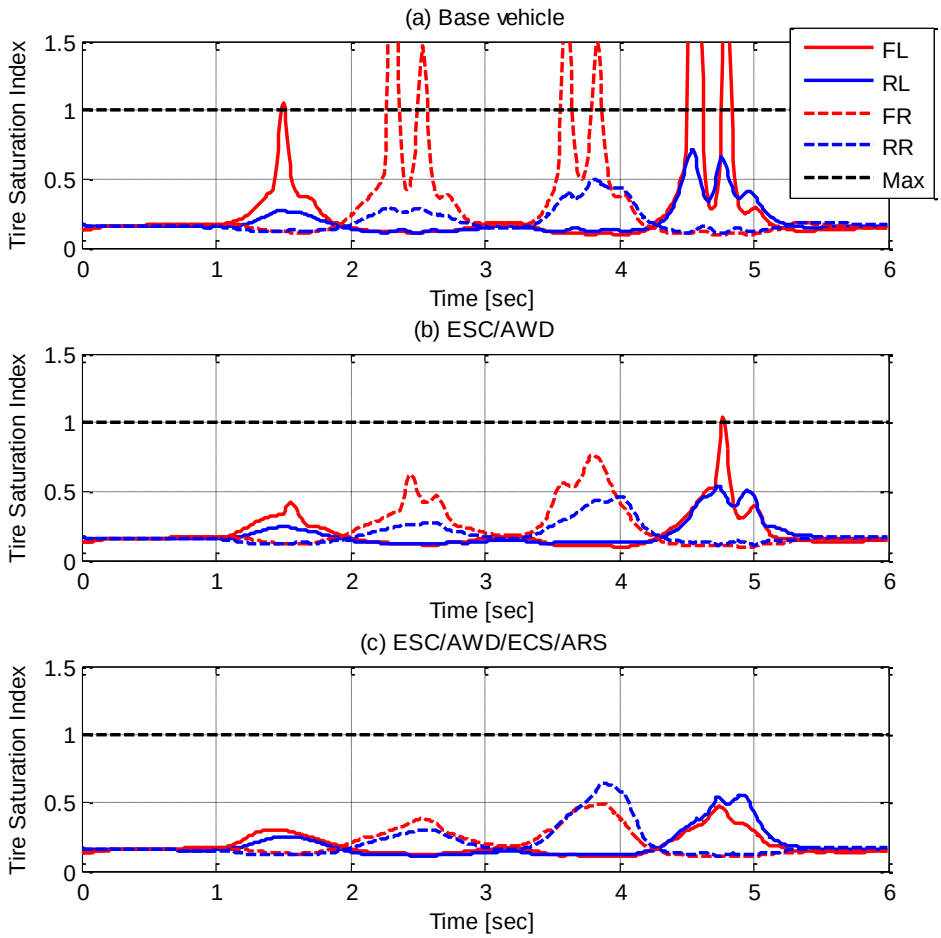

Figure 5.6. Tire saturation index at accelerating DLC

5.4.2. Closed-loop accelerating circular turning

In this scenario, the comparison the proposed ICC algorithm (4WD/ESC/ARS) with the ICC algorithm in [41] is conducted. The purpose of this scenario is to evaluate the performance of the proposed cost function and integration framework. The vehicle speed is set from 40kph to 100kph with constant 0.4g acceleration. Note that for fair comparison, ECS is not controlled in this simulation because effective integration of individual chassis module enhances the performance as seen in previous scenario.

The simulation result is shown in Fig. 5.7. As seen in Fig 5.7. (d), the lateral acceleration is nearly 1g(max : ~0.9g). The proposed algorithm well maintains steady state vehicle state even at the limit as seen in Fig 5.7. As seen in Fig 5.7. (a), within same time, travelling distance of the proposed ICC control system(234.4m) is larger than travelling distance of the ICC algorithm in [41](222.7m). This difference in travelling distance (11.7m) is equal to the 0.5sec difference in lap time. This difference results from the velocity tracking performance as seen in Fig 5.7. (c). Even though the upper level controller of the longitudinal force part is totally same, the tracking performance is different due to different cost function and integration framework. In lower level controller of [41], to avoid yaw

instability, the velocity tracking performance is compromised.

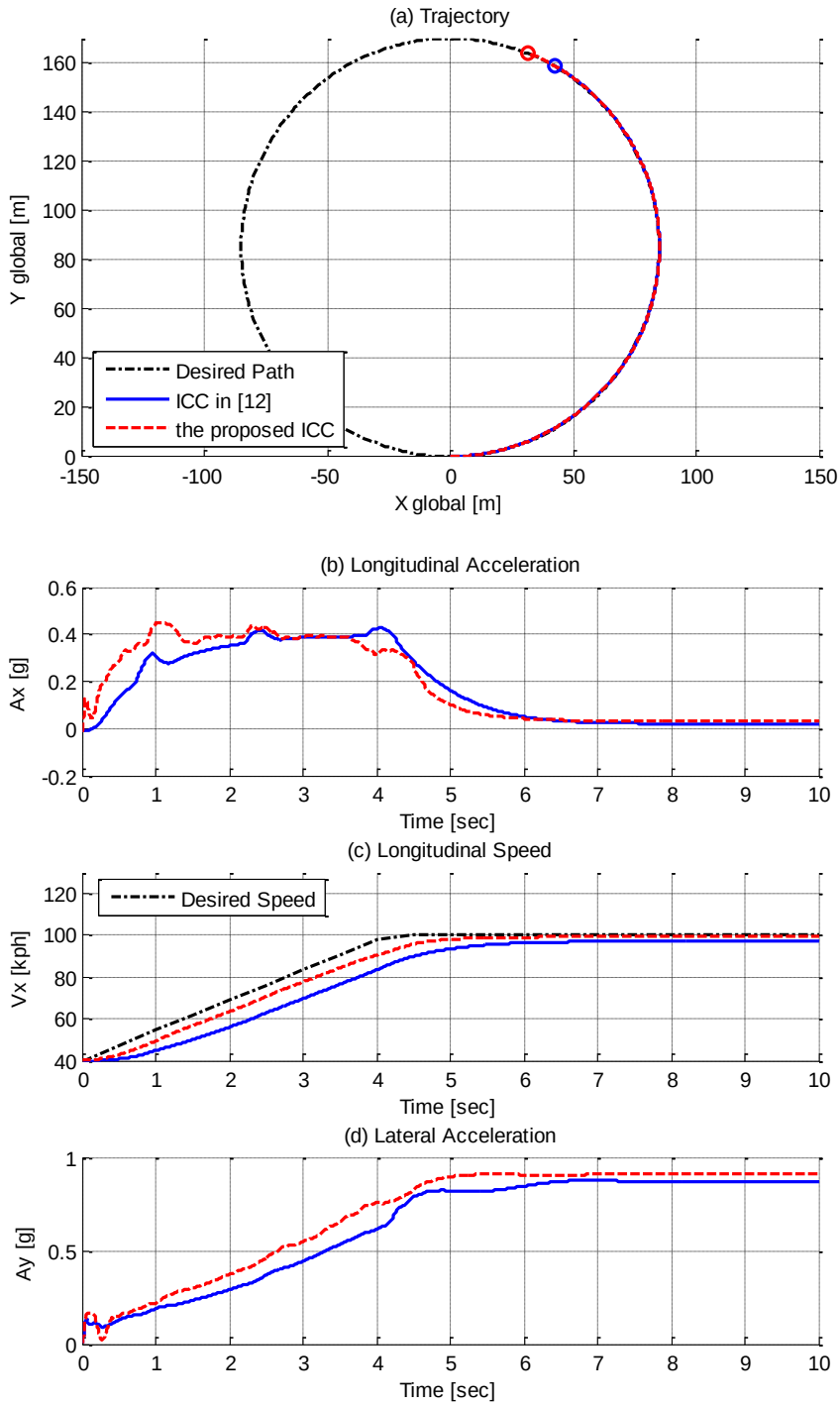

Figure 5.7. Overall vehicle performance at accelerating circular turning

Chapter 6

Vehicle Tests of 4WD/ESC/ECS Algorithm

To evaluate the performance of the proposed algorithm, vehicle tests have been conducted. The configuration of the test vehicle is shown in Fig. 6.1. The test vehicle is developed for vehicle chassis validation. The test vehicle has three chassis modules – 4WD : Front/Rear traction distribution / ESC : Four Independent wheel brake / ECS : Four suspension damping coefficient. Microautobox is implemented to control the vehicle and RT 3002 is employed to measure vehicle states.

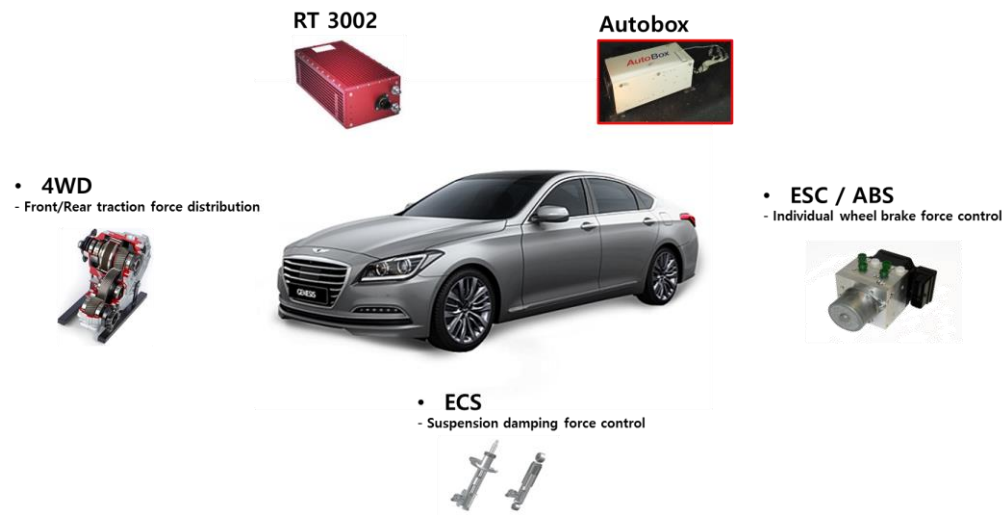

Figure 6.1. Configuration of Test Vehicle

The vehicle is luxury sedan. The test scenario is closed loop double lane change (DLC). This scenario is conducted on dry, asphalt road and driver conducts double lane change in constant speed, 80kph. In this scenario, the proposed ICC(4WD/ESC/ECS) algorithm is compared to base vehicle to evaluate effectiveness of integration of individual chassis module. Note that maximum brake pressure for ESC is limited to 15 bar due to actuator limitation.

6.1. Experimental Results

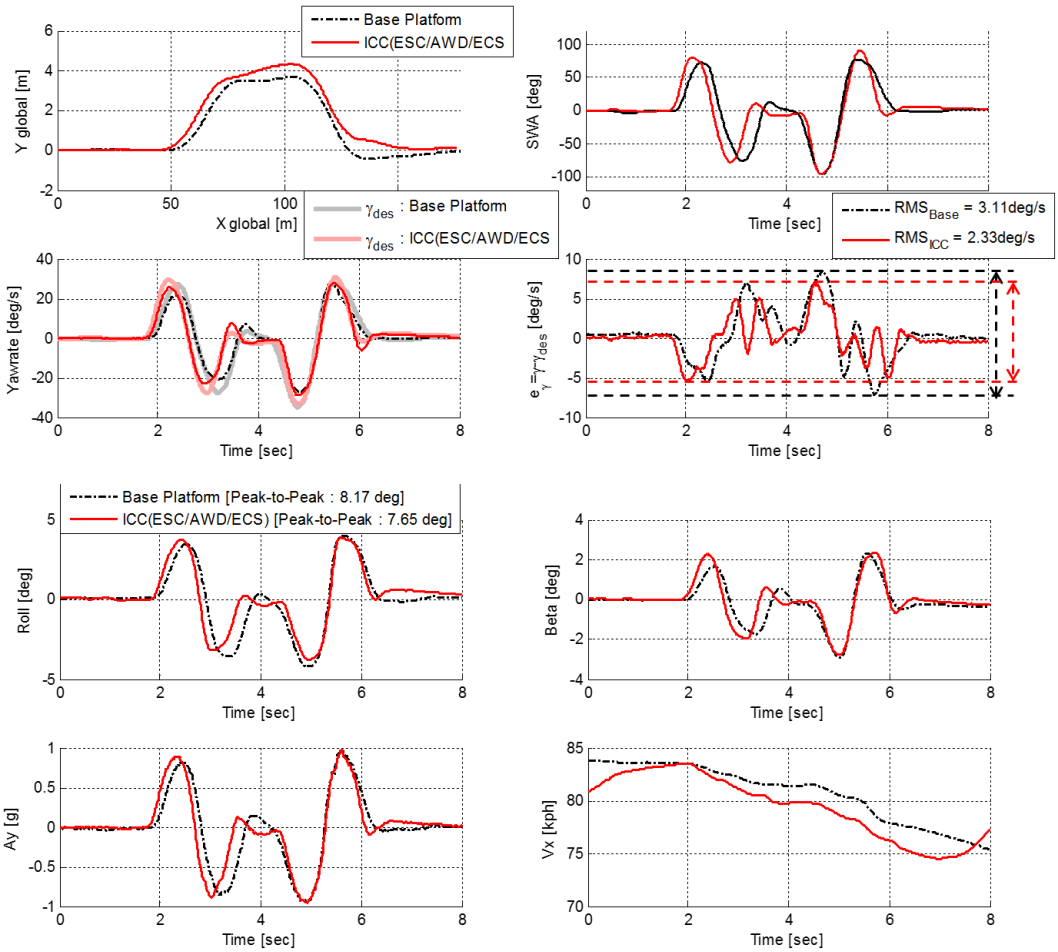

Figure 6.2. Overall vehicle performance at 80kph double lane change

The vehicle performance is validated via vehicle tests. Test scenario is 80kph double lane change (DLC) and the vehicle tests are conducted with luxury sedan of 2000kg weight. The results are shown in Fig.6.2. Steering wheel angle cannot be exerted identically unlike simulation results because the scenario is taken in closed loop by a driver. As seen in the Fig. 6.2, the ICC equipped vehicle reduces yaw rate error compared to base vehicle even at the limits as seen in lateral acceleration results.

Chapter 7

Conclusion & Future Works

A tire slip based integrated chassis control (ICC) algorithm of four-wheel drive(4WD)/ electronic stability control(ESC)/electronic controlled suspension(ECS) for enhanced limit handling is presented in this paper. Various simulations and vehicle experiments are conducted to validate and to compare the proposed ICC(Integrated Chassis Control) with other ICCs, the base model, and the ESC-equipped system.

The proposed algorithm consists of the following three parts: 1) a supervisor determines the desired dynamics from vehicle states and driver commands; 2) an upper level controller determines the desired force and moment to track the desired state based on the sliding mode controller; and 3) a lower level controller optimally allocates virtual control inputs, desired force and moment, to actual actuator control commands to minimize the performance index.

The performance index is newly proposed with the allocation guideline by using the sub-optimal solution and tire saturation penalty by monitoring the combined slip in this paper. To avoid nonlinearity of optimization procedure, the lower level controller consists of longitudinal(4WD/ESC) and vertical(ECS/ARS) tire force control allocation. The main concept of the control allocations are management of tire saturation penalty. In 4WD/ESC control allocation part, the sum of the tire saturation penalty is minimized. In contrast to longitudinal force control allocation part, the variance of the tire saturation penalty is minimized due to constant sum of the vertical force.

The proposed algorithm has been investigated via computer simulation. It has been shown that the proposed algorithm keeps stability and maneuverability at the limits by well management of tire saturation of four tires. By comparison the proposed system(4WD/ESC/ECS/ARS) with base model and 4WD/ESC equipped system, proposed cost function scheme is effective on integrating individual chassis modules. By comparison the proposed ICC algorithm with another ICC algorithm, proposed integration framework and cost function effectively increase maneuverability and guarantee stability.

The proposed algorithm has been investigated in target vehicle with 4WD/ESC/ECS. Compared to base vehicle, ICC equipped vehicle reduces yaw rate error even at the limits. This yaw rate tracking performance at the limits can be ensured safety when drivers encounter the possibility of lateral instability.

However, there are many possibilities for future research.

1. **Real-time tire parameter identification and friction estimation**

   Although tire parameters dominate the vehicle dynamics, reliable tire parameter identification method is still challenging tasks and research topics of many researchers. Varying road condition also affects to vehicle dynamics as well as tire parameter. In particular, road friction represents maneuver limits. If real-time tire parameter identification and friction coefficient estimation are achieved, integrated chassis control algorithm can cope with varying tire parameter and road condition appropriately.

2. **Excessive brake usage**

   To correct yaw rate error between vehicle yaw rate and desired yaw rate, brake is frequently used in this algorithm. Even though the excessive use of brake can achieve yaw rate tracking performance, longitudinal performance of the vehicle can be interrupted. Thus, minimization of brake use to maintain actual yaw rate in the vicinity of the desired yaw rate is important.

3. **Allocation guideline for ECS/ARS**

   The allocation guideline of the AWD/ESC provide the optimal solution which is robust and consistent against weighting gain and simulation case. However, the allocation guideline for ECS and ARS is not studied. By using allocation guideline for ECS and ARS, the robust performance can be achieved.

4. **Paradigm of integrated chassis control with ESC : Yaw rate tracking**

   Previous integrated chassis algorithms are aimed to track pre-defined desired yaw rate based on model. To blindly track desired yaw rate, the brakes of ESC are excessively used. However, unlike control algorithm, drivers cannot know desired yaw rate and only percept excessive deceleration by use of brake and discomfort. Thus, additional research on the design of integrated chassis control objectives are needed.

The development of the integrated chassis algorithm for limit handling of the vehicle will lead the increment of maneuver region and guarantee stability of the vehicle at the emergency situation, such as collision avoidance.

Bibliography

[1] B. Olofsson, K. Lundahl, K. Berntorp and L. Nielsen. "An investigation of optimal vehicle maneuvers for different road conditions." 7th IFAC Symposium on Advances in Automotive Control. 2013.

[2] J. Edréna, M. Jonasson, J. Jerrelind, A. S. Trigell and L. Drugge. "Utilisation of optimisation solutions to control active suspension for decreased braking distance." Vehicle System Dynamics ahead-of-print (2015): 1-18.

[3] R. de Castro, M. Tanelli, R.E. Araújo and S.M. Savaresi. "Minimum-time manoeuvring in electric vehicles with four wheel-individual-motors." Vehicle System Dynamics 52.6 (2014): 824-846.

[4] B. Li, A. Goodarzi, A. Khajepour, S. Chen and B. Litkouhi. "An optimal torque distribution control strategy for four-independent wheel drive electric vehicles." Vehicle System Dynamics ahead-of-print (2015): 1-18.

[5] A.K. Madhusudhanan, M. Corno and E. Holweg. "Lateral vehicle dynamics control based on tyre utilization coefficients and tyre force measurements." Decision and Control (CDC), 2013 IEEE 52nd Annual Conference on. IEEE, 2013.

[6] P. Song, M. Tomizuka and C. Zong. "A novel integrated chassis controller for full drive-by-wire vehicles." Vehicle System Dynamics 53.2 (2015): 215-236.

[7] R. Wang, C. Hu, Z. Wang, F. Yan and N. Chen. "Integrated optimal dynamics control of 4WD4WS electric ground vehicle with tire-road frictional coefficient estimation." Mechanical Systems and Signal Processing 60 (2015): 727-741.

[8] W. Cho, J. Choi, C. Kim, S. Choi and K. Yi. "Unified chassis control for the improvement of agility, maneuverability, and lateral stability." Vehicular Technology, IEEE Transactions on 61.3 (2012): 1008-1020.

[9] D. Li, S. Du and F. Yu. "Integrated vehicle chassis control based on direct yaw moment, active steering and active stabiliser." Vehicle System Dynamics 46.S1 (2008): 341-351.

[10] S. Chang and T.J. Gordon. "Model-based predictive control of vehicle dynamics." International Journal of Vehicle Autonomous Systems 5.1 (2007): 3-27.

[11] Macadam, Charles C. "Understanding and modeling the human driver." Vehicle System Dynamics 40.1-3 (2003): 101-134.

[12] Li, H-Z., et al. "Comprehensive lateral driver model for critical maneuvering conditions." International Journal of Automotive Technology 12.5 (2011): 679-686.

[13] Ungoren, Ali Y., and Huei Peng. "An adaptive lateral preview driver model."Vehicle system dynamics 43.4 (2005): 245-259.

[14] Bodie, M.O., and Hac, A., "Closed loop yaw control of vehicles using magneto-rheological dampers," No. 2000-01-0107. SAE Technical Paper, 2000

[15] Kritayakirana, Krisada, and J. Christian Gerdes. "Using the centre of percussion to design a steering controller for an autonomous race car." *Vehicle System Dynamics* 50.sup1 (2012): 33-51.
[16] Rajamani, Rajesh. Vehicle dynamics and control. Springer, 2011.
[17] Velenis, Efstathios, Panagiotis Tsiotras, and Jianbo Lu. "Optimality properties and driver input parameterization for trail-braking cornering." *European Journal of Control* 14.4 (2008): 308-320.
[18] Bentley, Ross. Speed secrets: Professional race driving techniques. MotorBooks International, 1998.
[19] Talvala, Kirstin LR, Krisada Kritayakirana, and J. Christian Gerdes. "Pushing the limits: From lanekeeping to autonomous racing." Annual Reviews in Control35.1 (2011): 137-148.
[20] Slotine, Jean-Jacques E., and Weiping Li. Applied nonlinear control. Vol. 199. No. 1. Englewood Cliffs, NJ: Prentice-Hall, 1991.
[21] Rossetter, E. J., J. P. Switkes, and J. C. Gerdes. "Experimental validation of the potential field lanekeeping system." International journal of automotive technology 5.2 (2004): 95-108.
[22] Lopez, Carl. Going faster!: mastering the art of race driving. Bentley Publishers, 2001.
[23] Thrun, Sebastian, et al. "Stanley: The robot that won the DARPA Grand Challenge." Journal of field Robotics 23.9 (2006): 661-692.
[24] Nagy, Bryan, and Alonzo Kelly. "Trajectory generation for car-like robots using cubic curvature polynomials." Field and Service Robots 11 (2001).
[25] Kang, Juyong, et al. "Design and testing of a controller for autonomous vehicle path tracking using GPS/INS sensors." Proceedings of the 17th IFAC World Congress, Seoul, Korea. 2008.
[26] S.H. You, J.S. Jo, S. Yoo, J.O. Hahn and K.I. Lee. "Vehicle lateral stability management using gain-scheduled robust control." Journal of Mechanical Science and Technology 20.11 (2006): 1898-1913.
[27] G. Phanomchoeng, R. Rajamani and D. Piyabongkarn. "Real-time automotive slip angle estimation with nonlinear observer." American Control Conference (ACC), 2011. IEEE, 2011.
[28] M. Gadola, D. Chindamo, M. Romano and F. Padula. "Development and validation of a Kalman filter-based model for vehicle slip angle estimation." Vehicle System Dynamics 52.1 (2014): 68-84.
[29] J. Dakhlallah, S. Glaser, S. Mammar, and Y. Sebsadji "Tire-road forces estimation using extended Kalman filter and sideslip angle evaluation." American Control Conference, 2008. IEEE, 2008.
[30] H.B. Pacejka. "Tire and vehicle dynamics." Society of Automotive Engineers., Inc., Warrendale, USA (2002).
[31] C. Ahn, H. Peng and H.E. Tseng. "Robust estimation of road friction coefficient using lateral and longitudinal vehicle dynamics." Vehicle System Dynamics 50.6 (2012): 961-985.

[32] R.Y. Hindiyeh, “Dynamic and control of drifting in automobiles.” Ph.D. dissertation, Stanford University, 2013
[33] A.E. Xavier. "Hyperbolic penalty: a new method for nonlinear programming with inequalities." International Transactions in Operational Research 8.6 (2001): 659-671.
[34] J. Wang. “Coordinated and reconfigurable vehicle dynamics control.” Ph.D. dissertation, The University of Texas at Austin, 2007
[35] O. Haarkegard. “Efficient active set algorithms for solving constrained least squares problems in aircraft control allocation.” Technical report LiTH-ISY-R-2426, Dept. of Electrical Engineering, Linkopings University, Sweden, 2002.
[36] http://www.koreacircuit.kr/, 2016.2.15
[37] Mejia, Juan Pablo Samper, Paul A. Theodosis, and J. Christian Gerdes. "Using a Path-Fitting Algorithm to Analyze the Racing Techniques of a Skilled Driver.“ ASME 2013 Dynamic Systems and Control Conference. American Society of Mechanical Engineers, 2013
[38] E. Velenis, and P. Tsiotras. "Optimal velocity profile generation for given acceleration limits: theoretical analysis." system 2 (2005): 5.
[39] Chu, T.W., and Jones, R.P., "Analysis and simulation of nonlinear handling characteristics of automotive vehicles with focus on lateral load transfer." Vehicle System Dynamics 46.S1 (2008): 17-31. doi: 10.1080/00423110701882272.
[40] Bodie, M.O., and Hac, A., "Closed loop yaw control of vehicles using magneto-rheological dampers," No. 2000-01-0107. SAE Technical Paper, 2000.
[41] Heo, H., Joa, E., Yi, K., and Kim, K., “Integrated Chassis Control for Enhancement of High Speed Cornering Performance." SAE International Journal of Commercial Vehicles 8.2015-01-1568 (2015): 102-109.

초 록

극한 주행 성능 향상을 위한 타이어 슬립 정보 기반 통합 샤시 제어 알고리즘

이 논문은 극한 주행 성능 향상을 위한 타이어 슬립 정보 기반 4륜구동(4WD)/ 차량 자세 제어 장치 (ESC)/ 전자식 제어 서스펜션 (ECS)의 통합 샤시 제어 알고리즘에 대해 서술했다. 극한 주행을 위한 차량 동역학 제어 알고리즘의 주된 목적은 극한 상황에서도 민첩하고 안정적인 거동을 보여 차량의 거동 가능 영역을 확장시키는 데에 있다. 이러한 목적을 성취하기 위해서 본 논문에서 제시한 통합 샤시 제어 알고리즘은 크게 3가지 구조 –Supervisor, 상위제어기, 하위제어기- 로 구성되어 있다. Supervisor는 차량의 상태와 운전자의 제어입력에 기반해 차량의 목표 거동을 설정한다. 상위제어기에서는 목표 거동을 추종하기 위한 종방향 힘, 요 모멘트, 필요에 따라서는 롤 모멘트를 계산한다. 하지만, 이렇게 계산된 힘과 모멘트를 어떻게 분배하느냐에 따라서 차량의 거동에 영향을 준다. 따라서, 하위 제어기에서는 이렇게 계산된 힘과 모멘트를 각각 액츄에이터에 극한 주행 성능 향상을 목적으로 분배한다. 개발된 통합 샤시 제어 알고리즘은 극한 주행 운전자를 모사하기 위해 개발된 운전자 모델을 활용한 폐루프 시뮬레이션과 차량 실험을 통해 검증되었다. 시뮬레이션 결과와 차량 실험을 통해 극한 상황에서도 향상된 극한 주행 성능을 보이는 것을 확인할 수 있었다.

키워드 : 통합 샤시 제어, 극한 주행, 타이어 슬립, 접선 경로 추종 오차
학번 : 2014-22505